PERFORMANCE ASSESSMENT OF MODEL ORGANIC RANKINE CYCLE POWER PLANT COMPONENETS FOR APPLICATION AT OLKARIA-I GEOTHERMAL POWER PLANT

HAILE ARAYA NIGUSSE

MASTER OF SCIENCE
(Mechanical Engineering)

JOMO KENYATTA UNIVERSITY OF
AGRICULTURE AND TECHNOLOGY

2014

Performance Assessment of Model Organic Rankine Cycle Power Plant Components for Application at Olkaria-I Geothermal Power Plant

Haile Araya Nigusse

A thesis submitted in partial fulfillment for the of Degree of Master of Science in Mechatronic Engineering in the Jomo Kenyatta University of Agriculture and Technology

2014

DECLARATION

This thesis is my original work and has not been presented for a degree in any other University.

Signature:..... Date.....

Haile Araya Nigusse

This thesis has been submitted with our approval as the university supervisors.

Signature:..... Date.....

Dr. Eng. Hiram M. Ndiritu

JKUAT, Kenya

Signature:..... Date.....

Dr. Robert Kiplimo

JKUAT, Kenya

DEDICATION

With praises to the 'creator of the universe', I dedicate this work to my loving family. A special feeling of gratitude to my loving and hard working mother, Hiryti Ghide, who saw the little light of hope in a period of destitution. Her words of encouragement ring in my ears. To my father Araya Nigusse, my sister Semhar who has never left my side and my brothers Habtom and Amanuel, thank you for your unconditional support with my studies. I also dedicate this work to my many friends.

ACKNOWLEDGEMENTS

First and foremost, praise and thanks to the almighty God for providing the opportunity and granting me the capability to proceed successfully. I would like to sincerely thank my supervisors Dr. Eng. Hiram Ndiritu and Dr. Robert Kiplimo who were more than generous with their expertise and precious time. My sincere thank for their guidance and encouragement throughout my entire study. I would like to express my most sincere gratitude to the Government of Eritrea and ADB (African Development Bank) through the National Board for Higher Education for sponsoring my Master of Science studies at Jomo Kenyatta University of Agriculture and Technology (JKUAT).

I would like to acknowledge and thank the management of the Olkaria I geothermal power plant for allowing me to conduct my research at their premises, their hospitality and cooperation in providing assistance as requested. My special thanks go to Mr. Dickson Katiwa Munyoki (MSc), Senior Drilling Engineer, Kenya Electricity Generating Co. Ltd (KenGen) for his continued support. I want to express my gratitude to the board of postgraduate studies of the School of Mechanical, Manufacturing and Materials Engineering. I appreciate their time devoted to reading and evaluating this work. Finally I would like to thank all my colleagues, staffs and technologists of the department of mechanical engineering and Engineering workshops (JKUAT)especially Mr. Daniel Kariuki, Mr.Masinde D., Mr. Mwai and Mr. Mugai that assisted me with this work. Furthermore, I would like to thank my family and friends for their limitless encouragement, support, love and care.

TABLE OF CONTENTS

LIST OF TABLES

LIST OF FIGURES

LIST OF APPENDICES

ABBREVIATIONS

PPM	Part(s) per million
IPP	Independent Power Producer
TDS	Total Dissolved Solids
NCGs	Non-Condensable Gases
ORC	Organic Rankine Cycle
DCSS	Distillation and Condensation Sub-System
KenGen	Kenya Electric Generating Company
COP	Coefficient of performance

NOMENCLATURE

η	Efficiency
ξ	Slope of working fluid on T-s diagram
Δ	Change
ρ	Density
n	Number of tubes
P	Pressure
r	Radius
T	Temperature
s	Entropy
th	Thermal
h	Enthalpy
c	Specific heat capacity
$\dot{w}$	Power
$\dot{m}$	Mass flow rate
$\dot{Q}$	The rate of heat transfer
$\dot{E}$	Total heat(energy) transfer
U	Overall heat transfer coefficient
d	Diameter
k	Thermal conductivity
R	Thermal resistance
W	Work

Subscripts

t	Turbine
tb	Tube
h	Hot
c	Cold
i	In
o	Out
r	Relative
w	Tangential
f	Axial
LMTD	Log mean temperature difference
cf	Counter flow

ABSTRACT

Energy consumption is an indispensable component for the continued development of the human population. Developing countries have higher economic growth rates and hence the energy consumption rate increases. Kenya is among the fast developing countries. According to the Kenya National Bureau of Statistics report 2012, the electricity consumption of the country has increased by over 5900 GWh in the years 2008 to 2011. The increase in energy demand, high cost of fossil fuels and the link between energy utilization and environmental impacts have resulted in the need for a sustainable approach to the utilization of the earth's energy resources. The Olkaria I geothermal power plant in Kenya uses a single flash condensing turbine type which constitutes three units each with a capacity of 15 MW. Moreover the plant does not operate at its full capacity. Reports on the available energy analysis of the power plant indicated that more than 17 MW power is lost as thermal energy. Currently, the hot water (brine) from the steam separator of the power plant is discharged to the surrounding while still at high temperatures and high pressure in which a significant amount of available energy is lost.

Despite the simplicity and low cost, a single flash steam geothermal power plant has the lowest efficiency mainly due to the untapped available energy in the brine. In Olkaria-I geothermal power plant the discharged brine has a temperature of 160^{o}C and mass flow rate of 197 metric tons per hour at an average pressure of 7 bars. This rejected high temperature brine results in wastage of significant amount of available energy which warrants further investigation to develop mechanisms for energy recovery. Moreover, the Organic Rankine Cycle (ORC) power plant is an advantageous technology that has been applied in generation of power from low temperature brine of geothermal reservoirs but has not been used at Olkaria-I. The power plant utilizes

a low boiling organic working fluid such as a refrigerant or a hydrocarbon. Researches indicated that the performance of ORC power plant is highly dependent upon factors such as proper organic working fluid selection, types of heat exchangers (condenser and evaporator) and turbine used. Despite a high pressure drop, shell-tube heat exchangers have satisfactory performance for ORC power plants.

The project involved the design, fabrication and performance assessment of the components of a model Organic Rankine Cycle power plant to utilize the geothermal brine at Olkaria I geothermal power plant. Two shell and tube heat exchangers (evaporator and condenser) and a single stage impulse turbine have been designed, fabricated and the performance assessment of each component has been conducted. The interacting fluids in the heat exchanger were pentane as a working fluid and hot water simulating the geothermal brine. The performances of the heat exchangers were evaluated in terms of the overall heat transfer coefficients in the flow streams, heat energy transferred and pressure drops across the heat exchangers. The turbine was coupled to a car alternator and the performance was evaluated in terms of shaft speed (RPM) and power generated using compressed air at different pressures to the inlet.

The results of the experiment indicated that the increase in mass flow rate of hot water by 0.08 kg/s caused a rise in overall heat transfer coefficient of the evaporator by 17.33% and the heat transferred was increased by 6.74%. In the condenser, the increase of cooling water flow rate from 0.15 kg/s to 0.35 kg/s increased the overall heat transfer coefficient by 1.21% and heat transferred was increased by 4.26%. Moreover, the performance of the single stage impulse turbine was tested using compressed air at different pressures. The shaft speed varied from 1585 to 4590 rpm as inlet pressure was varied from 0.5 to 5.0 bar and power generated was varying from 4.34 to 14.46 W. The results of the experiments indicated that the performance of each component

of the model Organic Rankine Cycle power plant operating at low temperature heat resources was satisfactory. It is anticipated that, an optimum design of an ORC will help increase the second law efficiency of existing open geothermal power plants. This will be recovery of low grade heat before re-injection of the geo-fluid back to the earth.

CHAPTER ONE

1.0 INTRODUCTION

1.1 Background

The global energy demand is expected to increase by over one-third in the period between 2012 to 2035 due to growth in economies and population [1]. This prevailing increase in energy demand will occur mainly in developing countries, where economic growth rates are high and more people are moving away from rural areas into the cities. Inhabitants of the rural areas are also shifting from biomass energy sources like wood and agricultural waste to electricity. However, most electrical power is currently generated from conventional power plants that utilize nonrenewable energy resources. As the electrical power generation increases, so do harmful combustion byproducts and biospheric contamination resulting to global warming [2].

Despite the high energy demand, the conventional energy resources such as fossil fuels and hydro resources have been declining due to depletion of the natural resource and drought. In addition, energy-related carbon dioxide (CO_2) emission is estimated to rise by 19% in 2035, resulting in a long-term average temperature increase of 3.6^oC [1]. The increase in energy demand, decline in energy resources and the environmental impacts have resulted in the search for a sustainable approach to the development and management of the earth's energy resources [3]. Geothermal energy is energy derived from the natural heat of the earth. The heat from the earth's own molten core is conducted to the adjacent rocks and transferred to underground water reservoirs by convection. The steam (hot water) heated by the geothermal heat can be tapped using different technologies. Geothermal energy is among the most reliable forms of renewable energy. Most of the other renewable energy sources such as hydro power are

weather dependent [4].

The carbon dioxide (CO_2) emission of an open loop system geothermal power plant is less than 4% of what is typically released by coal and other fossil fuel power plants. In a closed loop system geothermal power plant, there is no CO_2 emission [5]. For this reason it will be the future source of energy in most of the Eastern African countries especially those located within the East African Great Rift Valley region. This will reduce energy-related carbon dioxide (CO_2) emission and dependence on fossil fuel, hence address the global warming problem [4]. Geothermal energy resources are mainly categorized as steam-dominated and water-dominated. The medium and low-temperature water-dominated systems, mainly at a temperature range of 110 to 160^{o}C, are the most abundant [6].

It is however, important to note the limitations of geothermal energy conversion systems. Most geothermal power plants still operate on an open system. The loss of hot water in the process causes a gradual depletion of the reservoir. In addition to this, conventional geothermal power plants operate at low efficiency (from 12 to 21%) for water dominated geothermal resources mainly due to the untapped available energy in the brine [7].

1.2 Problem statement

Energy consumption is an essential component for the continued development of the human population. The rate of energy consumption may be considered as an indication of the national economic growth. According to a report from the World Bank [8] developing countries' economic growth will accelerate from 4.8% in 2013 to 5.3% percent in 2014 and the energy consumption will also increase. Kenya is one of the fast

developing countries. The main sources of power generation for the year 2010 included hydropower (42%), thermal oil (37%), geothermal (19%), co-generation (1.0%), wind (0.2%) and 0.5% is imported from neighboring countries [9].

From the foregoing statement, it is evident that Kenya's heavy dependence on hydro power generation has made the country susceptible to climate change impacts, such as drought and erratic rainfall patterns. Kenya needs to develop a more resilient and stable supply of electricity, while rapidly developing its base load of power generation to meet the growing demand. Although it is easier to expand its fossil fuel-based thermal generation, Kenya's Vision 2030 strategy places priority on low-carbon power systems including renewable energy source development [10].

The Olkaria geothermal field is the most explored and developed geothermal field in Kenya. The drilling operation was begun in Olkaria East (Olkaria I) field that led to the establishment of three units in June 1981. The Olkaria I geothermal power plant is a single flash condensing turbine which constitute three units each of a capacity 15 MW. Moreover the plant does not operate at its full capacity. The available energy analysis done by Kwambai [3] on the power plant shows there is 11 MW thermal energy loss in the steam transmission system and 6 MW of thermal energy is wasted in the separated brine. The brine produced by the interconnected production wells is currently discharged to the open drains while still at high temperatures (greater than 160^{o}C), high pressure (6 to 9 bar) and at 197 tons/hr in which is a significant amount of available energy that is lost [11].

Considerable amount of brine, currently re-injected or released into open drains at high temperature and pressure contains about 3.5% of the total power generated and is untapped energy. However, no study has been done to recover the available energy lost in the discharged brine.

1.3 Objective

The main objective of this study is to develop components of an organic power cycle for recovery of waste heat from geothermal brine to increase the amount of generated power. To achieve the above objective, the study aims at attaining the following specific objectives:

1. To design a lab scale model Organic Rankine Cycle power plant to utilize waste brine for power generation.
2. To test the performance of the heat exchangers in the organic Rankine cycle power plant.
3. To test the performance of the turbine for application in the ORC power plant.

1.4 Justification

Increasing the power capacity of a geothermal power plant can be obtained in a cost effective manner by utilizing otherwise untapped geothermal energy, without drilling new production wells. Moreover, this re-powering also provides additional environmental benefits. The ability to increase power generation, by modest amounts can lead to significant increase in profitability for operating power plants [12–17]. Generation of electricity from low temperature geothermal heat sources with a temperature of about 100^oC and higher exists in many countries. Some examples are the power plants in Altheim, Austria, with a power generation of 1 MW and in Neustadt-Glewe, Germany, with a power generation of 0.2 MW [18].

Evidently, the available energy of the separated brine in Olkaria I geothermal power plant presents a potential for improvement. 6 MW of geothermal energy that is cur-

rently wasted in the separated brine, which is released at the wellheads, will be utilized by employing a binary cycle power plant to generate more electricity [3].

1.5 Outline of Thesis

The thesis is organized in five chapters. The current chapter is the introduction to this research which gives a general highlight of the energy crisis and need for waste energy recovery in Olkaria I geothermal power plant. The second chapter presents a critical literature review of the studies that have been done on optimization of low grade energy recovery systems and main components of the model organic Rankine cycle power plant.

Chapter 3 outlines the experimental set-up and the parameters measured to establish performance of the main components of the model organic Rankine cycle power plant. Chapter 4 contains the results obtained from assessment test of the main components of the model plant and discussion. Chapter 5 contains the conclusion deduced from the determined performance assessment test and recommendations for further work at the Olkaria I geothermal power plant.

CHAPTER TWO

2.0 LITERATURE REVIEW

2.1 Introduction

The word geothermal originates from two Greek words, "geo", meaning earth, and "thermos", meaning heat since it is power extracted from heat energy stored within the earth's crust. Geothermal energy originates from radioactive decay of minerals, and from solar energy absorbed at the surface. This energy has been utilized for bathing since paleolithic times and for space heating since ancient Roman times. Nowadays, it is used commercially for both power generation and direct applications such as heating swimming pools and baths or therapeutic use (balneology), space heating and cooling (including district heating), agriculture (greenhouse heating and crop drying) as well as providing heat for industrial processes [4].

Worldwide, geothermal power plants have a capacity of about 12 GW power generation as of 2013 [19], and in practice supply only about 0.3% of global power demand. In addition to the power generated, about 28GW geothermal energy is installed for direct applications like district heating, space heating, balneology, process heating in the textile industry, desalination, fish farming and agricultural applications. Recent technological advances have dramatically expanded the range and size of viable resources, especially for applications such as home heating, opening a potential for widespread exploitation [4].

Kenya is the first country to start exploiting the geothermal energy in Africa and has been exploiting the resource for the last 32 years [20]. Exploration was commenced in 1956 in the areas mainly located on the floor of the East African Great Rift Valley

region at a distance of about 120 km northwest of the capital city, Nairobi [21]. The estimated geothermal resource potential was about 7,000 to 10,000 MW in 2013. Out of these, only about 296 MW have been exploited [22].

The Olkaria geothermal field produces a two-phase mixture of steam and hot water in general proportions of 85% steam and 15% hot water which is a suitable resource for electrical power generation [23]. The Olkaria I power plant is a single flash steam geothermal power plant that is constituted of three units commissioned in 1981 to 1984 and each unit generates 15MW of electrical power. The two phase mixture of steam and hot water from the ground enters the steam separator where steam is separated from hot water by density difference and cyclone action. The steam is supplied to the turbine whereas the hot water (brine) is discharged to open drains [3]. The brine produced by the interconnected production wells is disposed at a temperatures of greater than 160^{o}C, pressure of 6 to 9 bars and mass flow rate of 197 tons/hr which contain about 3.5% of the total power generated and is untapped energy [11].

Moreover, Olkaria I was observed to have a declining steam production at a rate of 4% during the first 10 years of operation [24]. Consequently the capacity of the power plant was reduced from 45 to 30 MW. In order to restore the design capacity, make up wells were drilled and the declined wells were retired. Recently some of the retired wells in the Olkaria field are being used as injection wells [4]. However, drilling additional wells is not a sustainable approach to utilization of geothermal resources and may increase the possibility of local earthquakes [24].

Furthermore, in Olkaria I geothermal power plant, the brine produced by the interconnected wells is currently discharged into open drains at high temperature (more than 160^{o}C) which wastes a significant amount of available energy [11]. The available energy analysis done by Kwambai [3] on Olkaria I geothermal power plant indicated that

about 11 MW of power is lost during the steam transmission from the production wells to steam separator and about 6 MW power is lost in the discharged brine after steam separations. This suggests that causes of energy loss in steam transmission systems warrant further investigation in order to develop mechanisms of energy recovery.

2.2 Geothermal energy utilization

Geothermal energy has been exploited commercially for many years on a large scale both for electricity generation and direct use depending on the source temperature. The geothermal energy resources are mainly categorized as vapor-dominated, water-dominated and dry rock or magmatic [25]. In the vapor dominated reservoirs, although hot water and water vapor can co-exist, the vapor phase is the continuous phase determining the pressure regime of the reservoir. Larderello field in Italy and Geysers field in the USA are the best-known vapor dominated geothermal reservoirs. In the liquid dominated reservoirs, liquid is the continuous phase due to the high pressure. The hot water (brine) within these systems is known for the chemical solution containing sodium, potassium, lithium, calcium, chloride, bicarbonate, sulfate, borate and silica. Wairakei in New Zealand, Cerro Prieto in Mexico and Kizildere in Turkey are examples of liquid dominated reservoirs [26]. The heat recovery from liquid dominated reservoirs is higher compared to heat recovery from vapor-dominated reservoirs. The main reason of the higher heat recovery is the boiling of fluid in the reservoir.

Hot dry rock (HDR) or magmatic systems do not contain vapor or water reservoir. The heat of the magma is extracted by circulating a working fluid in the top part of the magma chamber. The heat transferred to the working fluid then is used to power a closed Rankine-cycle power plant [26].

The design of a power plant utilizing the geothermal heat resources depends on the availability and quality of the hot water. For a high temperature and high pressure steam-dominated geothermal resource, where the percentage of non condensing gases (NCG) concentration is low, the dry steam power plant is an advantageous means of power generation. Binary cycle power plants are more effective in utilization of low-intermediate temperature geothermal resources and high temperature resources containing a high percentage of NCG concentration [27]. Geothermal hot water (steam) contains NCGs such as CO_2, H_2S, NH_3, N_2, CH_4 and air. The concentration of NCGs can vary from less than 0.5% to greater than 25% by weight of hot water (steam). Some examples of geothermal fields that contain high NCG concentration are Kizildere, Turkey (10-21%), Larderello, Italy (10%) Broadlands, Ohaaki, New Zealand (3-6%), BacMan, Philippines (5%), Sibayak, Indonesia (3.1%), Tongonan, Philippines (3%), Geysers, USA (0.5-2%), Palinpinon, Philippines (1.3%) [28].

2.3 Geothermal power plant configuration

Three major types of geothermal power plants in operation are: Conventional power plants (dry steam and flash steam), binary cycle (Organic Rankine cycle and Kalina cycle) power plants and combined (flash/binary) power plants.

2.3.1 Conventional geothermal power plants

The dry steam geothermal power plants utilize steam at high pressure and temperature from the geothermal reservoir directly to generate power. Though the dry steam power plants are the simplest in construction and less costly, they are very rare due to the availability of natural dry steam geothermal resources. Natural dry geothermal steam

is unavailable in limited areas for example the Geysers in northern California (USA).

Flash steam power plants (single flash and double flash) utilize hot water from the deep production wells for power generation. The two-phase geo-fluid flows under high pressure maintaining a liquid state though the temperature is above the normal boiling point. Due to the pressure loss in the pipeline, hot water starts to boil and as the pressure is relieved further in a separator the hot water flashes into steam. Flash steam geothermal power plants are characterized by simple and low cost plants, though the geothermal resource is only partially utilized. The steam phase is used to drive the turbine/generator while it is augmented by several flash stages, all the remaining liquid phase (brine) is discharged into the re-injection well.

Bodvardson and Eggers [29] compared single flash and double flash geothermal power plants using their available energy at the same source and sink temperatures. They found that the second law efficiency of a double flash power cycle is greater than a single flash cycle by about 3%. A study by Lawrence [30] also indicated that though the cost of a double flash power plant is about 5% higher than a single flash, the output of the plant is increased by 20 to 25%.

Despite the simplicity and least cost, flash steam power plants have low efficiency mainly due to the untapped available energy in the brine. Injected brine generally has a temperature higher than 100^{o}C and mass flow rate of hundreds of tons/hour [31]. This rejected high temperature brine wastes significant amount of available energy and causes thermal pollution to the environment [32].

2.3.2 Binary cycle geothermal power plants

Binary cycle power plant is an advantageous technology that consents the thermal energy from low temperature water dominant reservoirs and makes geothermal power generation feasible even for countries lacking high temperature geothermal resources. In a low to moderate enthalpy resource, the steam quality is 10 to 30% based on fluid enthalpy and separation pressure [33]. The steam and hot water streams can be efficiently utilized in a two-phase Organic Rankine Cycle (ORC) unit. Separated steam (usually with some percentage of Non-Condensable Gases or NCGs) is introduced in the vaporizer to vaporize the organic working fluid. The geothermal condensate is mixed with the separated brine to provide the preheating medium of the organic fluid before being injected back to the ground. In such configurations, the geo-fluid remains confined and thus, environmental problems associated with the exploitation of geothermal resources, like the release of greenhouse gases (e.g. CO_2 and CH_4) and the discharge of toxic elements (e.g. Hg and As) are avoided. In addition to this, there is no direct contact between the geothermal fluids (or brine) and moving mechanical components of the plant (e.g. the turbine), assuring a longer life for the plant equipment [34].

Many researchers [35–38] showed that although a binary power plant utilizes a low temperature geothermal resource, the heat extracted from the steam is limited due to the silica scaling risk. A method to partially overcome the cooling temperature limit is to add a recuperator which recovers heat from the vapor exiting the turbine. However a recuperator is applicable when the organic fluid is of a dry expansion type, mainly a fluid where the expansion in the turbine is done in the dry superheated zone. The recuperated Organic Rankine cycle is typically 10-15% more efficient than the simple Organic Rankine cycle. Moreover, for low-temperature geothermal systems

which produce only hot water, the binary cycle geothermal power plants perform at low first law efficiencies (5-10%) and second law efficiencies (25-45%) range [39].

2.3.3 Organic Rankine Cycle power plant

The Rankine cycle is named in honor of one of the founding contributors to the science of thermodynamics; William John Macquorn Rankine (1820 - 1872), a Scottish engineer and physicist who is also credited for the 'Rankine' temperature scale. In a search for an alternative working fluid, Frank Ofeldt in 1883 developed a unique power system that uses naphtha (a distillation product from petroleum) as a working fluid [40]. The establishment of the Organic Rankine Cycle (ORC) was as a result of the need to utilize different low boiling point organic working fluids for low to medium temperature heat resources.

Recently, ORC has become a very attractive option of power generation from low-grade heat sources especially after the development of suitable working fluids to replace water in conventional Rankine cycle [41]. Energy conversion from low temperature heat sources becomes possible through the use of these organic working fluids, which are usually in the form of chloro-fluoro-carbons (CFC), hydro-chloro-fluoro-carbons (HCFC) and hydro-fluoro-carbons (HFC) [42].

An Organic Rankine Cycle (ORC) power plant is similar to a conventional steam power plant. However, it utilizes low boiling point organic working fluids such as refrigerants and hydrocarbons instead of water. In recent years, research has intensified on this power cycle as it is being progressively adopted as premier technology to generate electricity from low temperature heat resources [16, 17, 43].

Although an Organic Rankine Cycle power plant has been under research since the

1880s, it has never been a premier power cycle until recently. This is due to the growing concern over the future depletion of fossil fuels and global environmental destruction. Tchanche *et al.* [43] studied existing applications of binary cycle for geothermal power plants and biomass combined heat power (CHP) plant and analyzed their maturity. The study indicated that waste heat recovery organic Rankine cycle systems in the near future will experience a rapid growth. Organic Rankine cycle solar power plants are being intensely investigated at smaller scale for co-generation applications in buildings but larger plants are also expected in regions with constant and low solar radiation intensity.

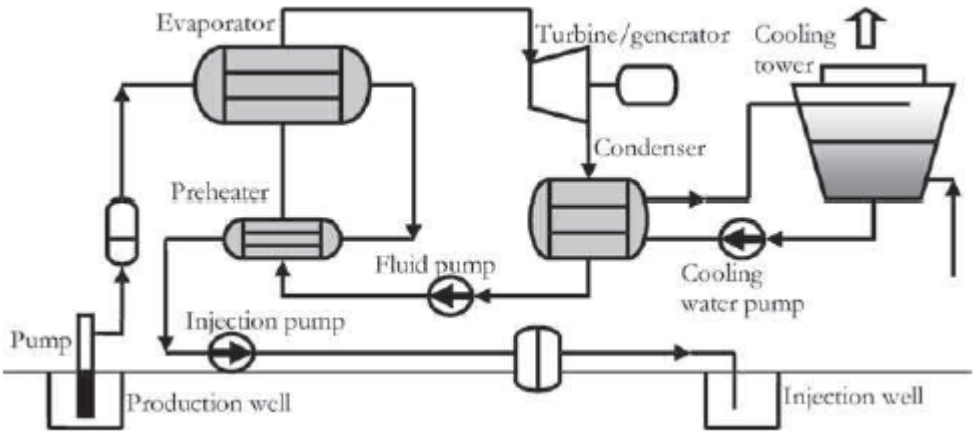

Figure 2.1: Flow diagram for ORC geothermal power plant [43].

The Organic Rankine Cycle power plant (Figure 2.1) proves to be a very promising technology for low to moderate temperature geothermal resources and a bottoming unit for heat energy recovery in conventional geothermal power plants. The cycle has advantages of low cost of maintenance operation, consumes nearly no additional fuel for the same added power output and would decrease the environmental pollution. However, the low temperature energy conversion efficiency was found to be 10-13% which is low compared to the high temperature energy conversion [44].

The applicability of ORC power plant depends upon many parameters such as proper

selection of organic working fluids, energy source temperature and its mass flow rate, type of heat exchangers (condenser and evaporator) used. These parameters are interdependent and the effectiveness of the cycle depends on the collective effect of each parameter on the cycle operation [45].

2.3.4 Typical Working fluids in ORC

Organic Rankine Cycle (ORC) power plants utilize a variety of working fluids. Among these are pentane, propane, toluene and ammonia. The organic working fluids have high vapor pressure and consequently low saturation temperature, hence effective low grade energy conversion would take place. Selecting a working fluid with a relatively high density at condenser temperature prevents the use of large turbines and condensers. Hence the use of multistage turbines is no longer needed [32].

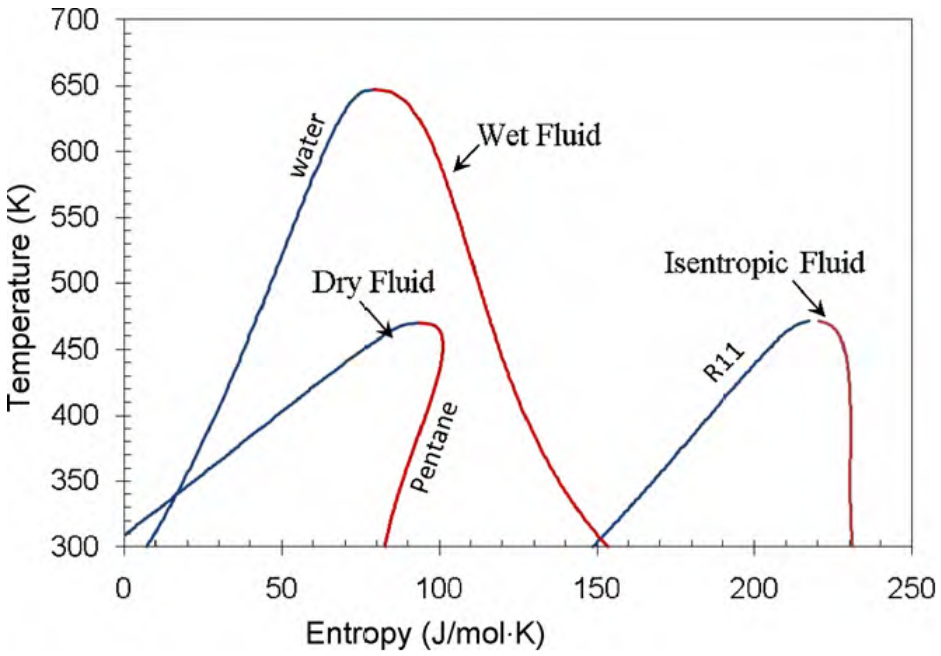

Figure 2.2: Three types of working fluids: dry, isentropic, and wet [46].

Chen *et al.* [46] studied several types of working fluids that included propyne, cy-

clopropane (HC-270), ethane (R-170), carbon dioxide (R-744), fluoromethane (R-41), trifluoromethane (R-23) etc, in an organic Rankine cycle. He found that working fluids with high density and high latent heat provide high unit turbine work output. When the working fluids are compared for example, at same pressure and temperature (1 bar and 25^{o}C), cyclopropane (HC-270) has the highest latent and density followed by propyne. The study also showed the slope of the saturation curve of a working fluid in a T-s diagram can be skewed to the right, left or non skewed as shown in Figure 2.2. The fluids are therefore referred to as wet, dry or isentropic fluids depending on the slope of the saturation vapor curve on a T-s diagram (dT/ds) (Figure 2.2). Wet fluids like water usually need to be superheated to avoid liquid droplet in the turbine during expansion as pressure drops, while many organic fluids, which may be dry or isentropic, do not need superheating. Though the study established some unique characteristics of organic working fluids, their environmental impact was not considered. It is therefore necessary to compare these findings with other organic working fluids.

Woodland *et al.* [47] also studied the performance of dry working fluids that included (R600a, n-Pentane and R245fa) in an organic Rankine cycle. They found that these fluids allow for zero superheat at the expander inlet which is the main advantage of these fluids at low heat source temperatures. Furthermore, they found n-pentane offers the best cycle efficiency of the working fluids studied.

DiPippo [48] compared ammonia-water mixture as a working fluid (Kalina cycle) and an organic working fluid (Organic Rankine Cycle) under identical conditions. Being a mixture, the working fluid did not have a constant boiling and condensing temperature. The phase change occurred at varying temperature range causing boiling to begin at low temperatures ($20 - 170^o$C) [49]. The study showed the Kalina cycle has 15-50% more power output and 3% increase in efficiency. Although the turbine power can be

increased, the cooling parasitic power increases to partially nullify the gain. This power includes the power consumed by the cooling system (cooling tower) and feed pump. The required condenser size may be increased because the condenser heat load will probably be increased [50]. Moreover, the Organic Rankine Cycle (ORC) is much less complex and needs less maintenance [48]. Thus Organic Rankine Cycle power plants are a promising technology from the perspective of investment costs and utilization of lower temperature geothermal resources.

2.3.5 Organic Rankine Cycle power plant heat exchangers

Heat exchangers are the most important components in an Organic Rankine Cycle power plant to facilitate energy transfer between the hot water (geo-fluid) and the organic working fluid. However, variation of parameters (such as mass flow rate, pressure drop, concentration of the geo-fluid) must be taken into account during design and material selection of the heat exchanger. Among the many categories of heat exchangers are plate, shell tube and shell coil heat exchangers.

Madhawa [51] investigated the flat plate and shell tube heat exchangers and found that flat plate type heat exchangers are effective in the evaporator and condenser when considering low-temperature geothermal heat sources in which large heat exchanger area (per unit power output) is required. The plate type heat exchangers are preferred due to their compactness and high heat transfer coefficients which result to less heat transfer area than would be needed using shell and tube heat exchanger. However, flat plate exchanger involves high manufacturing and maintenance cost. Hence it has significant effects the overall cost of the power plant.

Bambang [52] also compared the flat plate and shell tube heat exchangers and found

that the shell tube type is advantageous due to simplicity in geometry, well-established design procedure, can be constructed from a wide range of materials, uses well-established fabrication techniques and is easily cleaned. The shell tube heat exchanger can be designed and manufactured locally from a wide range of materials, but for low temperature heat resources, the plate heat exchangers are more effective. However, the heat transfer optimization is a key challenge mainly due to large pressure drops within the shell tube heat exchangers.

The design of a heat exchanger involves establishing the right flow pattern of the interacting fluids. Parallel and counter flows are the two common flow patterns in shell tube heat exchanger. The counter flow is the preferred flow pattern in liquid to liquid heat exchangers since it results in a higher temperature difference [53].

Various studies have been carried out on optimization of the performance of shell and tube heat exchangers using the performance parameters approach. The heat transfer coefficient values are evaluated using the log mean temperature difference (LMTD) method from the temperature difference and the heat transfer area for known inlet and outlet temperature of the heat exchangers [54]. Thundil *et al.* [55] investigated the effect of inclination of baffles in the shell by simulating a model shell and tube heat exchanger. This involved comparing the impact of baffle inclination on fluid flow, pressure drop and the heat transfer characteristics of a shell tube heat exchanger using three different inclination angles (0^o, 10^o and 20^o). They concluded that a shell and tube heat exchanger with 20^o baffle inclination angle has a better performance compared to 10^o and 0^o inclination angles.

In general, conventional shell tube heat exchangers result in high shell-side pressure drop and formation of re-circulation zones near the baffles. To overcome this challenge, helical baffles, which give better performance than single segmental baffles, can

be used. However, these baffles involve high manufacturing cost, installation cost and maintenance cost. It is therefore important that the cost of the exchanger be considered as well in the design [55].

2.3.6 The Organic Rankine Cycle (ORC) turbine

The turbine is a turbomachine which extracts the heat energy of vapor and transforms it into mechanical rotational energy or shaft work [56]. An improved design and materials selection of turbine components offers a cost effective and flexible maintenance service. The combined cycle power plant market demands constantly high performance, reliability and operating flexibility at moderate prices for competitive life cycle costs [57].

Multi stage turbines are used in conventional Rankine steam power plant because the pressure ratio and the enthalpy drop over the turbine are very high. However, in ORC cycles the enthalpy drop is much lower and hence a single or low number of stages in a turbine should suffice hence lowering the costs [58].

2.3.7 Combined cycle geothermal power plant

Combined geothermal power plants (Figure 2.3) incorporate both a binary cycle plant and a flashing power plant to exploit the advantages associated with both systems. Three common types of combined geothermal power plants are the brine bottoming binary system, exhausted steam bottoming binary system and the hybrid system. The brine bottoming binary system comprises a combination of a single flash condensing turbine plant and a binary cycle utilizing separated brine. The exhausted steam bot-

toming binary system consists of a combination of a single flash back pressure cycle and a binary cycle utilizing the turbine exhaust steam and the hybrid system consists of a combination of a single flash back pressure cycle and a binary cycle utilizing both separated brine and exhaust steam. [59].

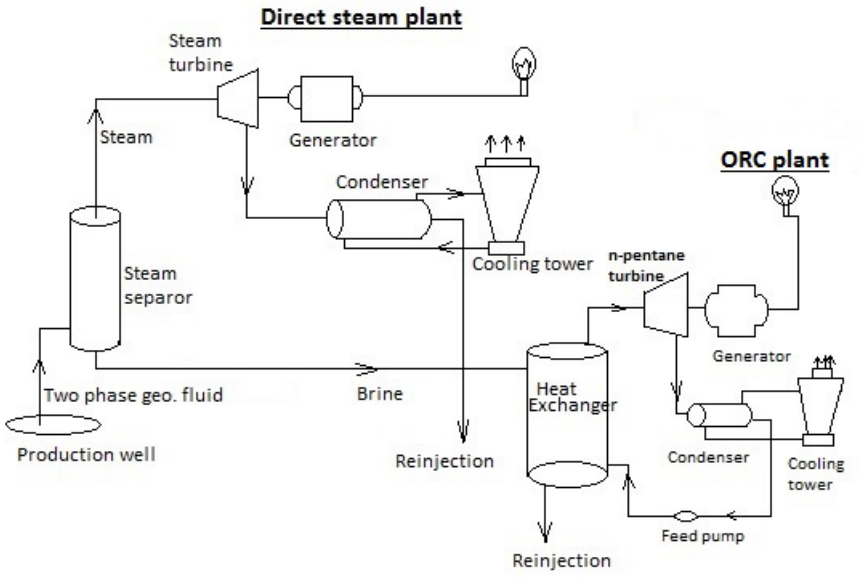

Figure 2.3: Direct steam (Single flashing) plant and binary cycle plant combined geothermal power plant [52]

.

Andi J. Nugroho [59] comparatively studied three types of combined cycle geothermal power plants at different geothermal resource temperatures and enthalpy. He found that for geothermal resource temperature above 240^{o}C, the hybrid system was economical and produces more power. For geothermal resources at a temperature of below 240^{o}C the brine bottoming binary system is more advantageous due to high specific power output production and the most economically viable option since it requires least total investment cost.

In the case of the geothermal fluid with excess enthalpy, the hybrid system was found to

be a superior power plant configuration due to higher specific power output. The system was a viable option for utilizing geothermal fluids with enthalpy below 1700 kJ/kg. At higher fluid enthalpy, the total capital investment cost was similar between the exhausted steam bottoming binary system and the hybrid system. In this study, only three configurations of combined geothermal power plants were considered. However the lower temperature limits of the power cycles and the optimum working conditions of each plant needs to be studied [59].

Though Bombarda *et al.* [60] found that the additional power generated is much lower than the base power, the combined geothermal power plants have significantly greater efficiencies due to higher overall utilization of geothermal resource and extraction of more power (heat) from the geothermal resource. However, the study did not consider the economic viability of the combined power plant and never compared the different configurations of combined geothermal power plant.

2.4 Utilization of geothermal energy in Kenya

2.4.1 Background

Kenya has prodigious potential of power generation from geothermal energy resources but it is not yet making full use of that potential. The most explored and developed geothermal field in Kenya is the Olkaria geothermal field. The field is divided into seven sectors to facilitate easier utilization and extensive drilling operations [20].

2.4.2 The Olkaria I geothermal power plant overview

The Olkaria I geothermal power plant has three single flash type units each at a capacity of 15 MW giving a total installed capacity of 45 MW. All units are products of Mitsubishi Heavy Industries, Japan. The first two units are identical in construction with most parts being interchangeable. The third unit, though based on the same design philosophy, has slightly improved parts which are not interchangeable with the initial two units according to the study done by Henry Wesula [61]. The study also suggested a more proactive steam field management regime to reduce the effects of well decline. However, the study revealed that no measures have been put in place to ensure fast reservoir recharge.

2.4.3 The Olkaria II geothermal power plant

The Greater Olkaria Field is being exploited and at least 202 MW of electric power is being generated from the field. The Olkaria II geothermal power plant with a capacity of 70 MW was commissioned in 2003. The plant is supplied with steam from twenty production wells. The total steam available from the North East (Olkaria II) production wells in 2004 could support generation power of 98 MW [62]. The availability of excess steam implies that the potential of the field is more than the current production. Plans are underway to increase the power plant output as evidenced by the drilling operations that are on-going [20].

The Olkaria I and II power plants are owned by KenGen. The Olkaria III area with a pilot 13 MW plant is owned by ORMAT (an IPP). Olkaria IV area (locally referred to as Domes) has three exploration wells drilled with temperature up to 350^oC. This area is now earmarked for appraisal and production drilling for a 70 MW power plant [63].

2.5 Project opportunities identified in from the study of literature

The following gaps have been identified from the literature review:

- Single flash geothermal power plants operate at low efficiency for a two phase geothermal resource and this is what is in use in Kenya.
- The energy loss in Olkaria I geothermal power plant warrants further investigation in order to develop mechanisms of energy recovery.
- The combined cycle geothermal power plants have significantly greater efficiencies yet they have not been exploited in geothermal power generation in Kenya.
- The Organic Rankine Cycle (ORC), another configuration of efficient geothermal power systems has also not been used at Olkaria I.
- The Organic Rankine Cycle power plant utilizing dry expansion working fluid is characterized by its robustness, compact design and higher efficiency and is not being utilized in Kenya.

CHAPTER THREE

3.0 METHODOLOGY

3.1 Background

The existing Olkaria I geothermal power plant is a single flash condensing turbine type that is constituted of three units each with a capacity 15 MW. Moreover, the plant does not operate at its full capacity. The available energy analysis done by Kwambai [3] on the power plant showed there was a total of 17 MW power losses in steam transmission systems and in the separated brine.

The brine produced by the interconnected production wells is currently discharged to the open drains while still at high temperatures (greater than 160^oC), high pressure (6 to 9 bar) and at 197 tons/hr in which a significant amount of available energy that is lost [11]. The untapped energy in the discharged brine is about 3.5% of the total power generated. Organic Rankine Cycle power plant is an advantageous technology that allows the power generation from low temperature water dominant geothermal resource.

In this study, the components of a model Organic Rankine Cycle power plant for recovery of waste heat from the geothermal brine to increase power generation were developed and performance assessment of each component was conducted. The model power plant utilizes hot water simulate the geothermal brine which is currently discharged to the surrounding.

The model power plant is shown in Figure 3.1. It consists of pentane as the main power generating fluid coupled to a hot water system that supplies energy to run the ORC. The hot water stream at a temperature of 54^oC was obtained from an electric water

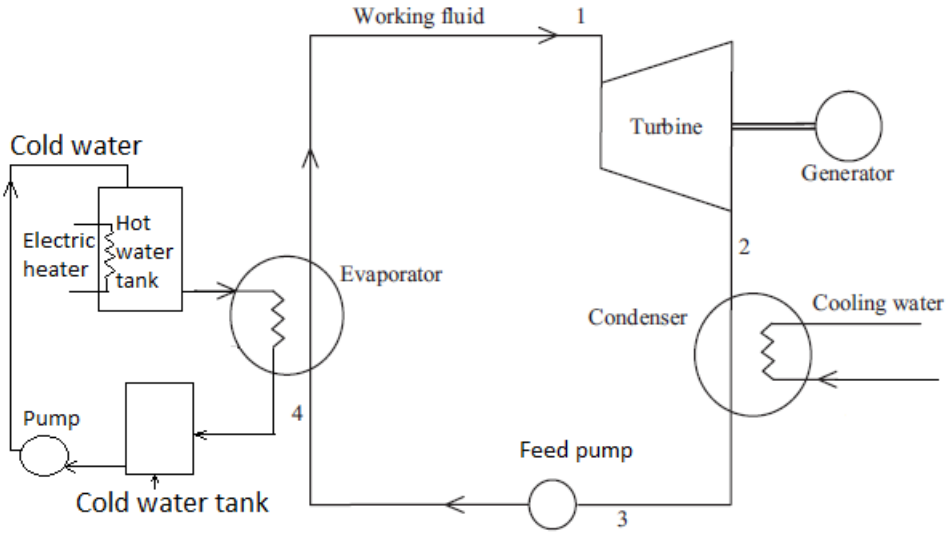

Figure 3.1: Schematic diagram of the Model Organic Rankine Cycle power plant

heater in the hot water tank. In the flow diagram shown on Figure 3.1, process 1-2 is the expansion of the working fluid in the turbine to produce mechanical shaft power. Process 2-3 represents the condensation of vapor in a water cooled condenser. Process 3-4, represents the pumping of the organic working fluid (n-pentane) to the evaporator and process 4-1 is vaporization of the working fluid in the evaporator.

The lab scale model organic Rankine Cycle power plant was designed to operate at a heat source temperature of 50 to 60^{o}C and pressure between 1 and 2.5 bars. Hot water simulating the geothermal brine was the main heat source of the model power plant. Moreover, availability and cost of materials, viability of the fabrication techniques of the main components, working fluid properties (saturation vapor curve, high stability temperature, low environmental impact and safety) were considered in the design. The details of the design of the power plant are presented in this chapter.

3.2 Working fluid selection

The thermodynamic and chemical characteristics of an organic working fluid greatly determines the output and performance of the Organic Rankine Cycle power plant. To utilize low temperature heat source effectively, the working fluid of the power cycle should possess low boiling temperature [46,64]. In this research, working fluid thermodynamic properties such as an appropriate evaporation and condensation properties, the temperature-entropy diagram and the chemical stability over the given temperature range were considered. Moreover, the non-thermodynamic properties, ecological and technological standards, safety requirements and cost were also imposed on the selection of the working fluid.

However, getting a working fluid that would satisfy all design requirements and does not have any disadvantages was impracticable. Therefore, it was meaningful to look at organic working fluids that possess the maximum advantages. In this model power plant pentane was selected as a working fluid. Though pentane is a highly flammable organic fluid, its physical state is convenient for thermodynamic cycle working between normal atmospheric condition and the boiling condition of water.

Pentane is a dry expansion working fluid that has saturated vapor curve skewed to the right which has the advantage that expansion always ends within the dry region. The use of dry expansion working fluid eliminates the danger of blade erosion and low maintenance operation is assured. In general, the ORC that utilizes a dry expansion working fluid is characterized by its robustness, compact design and a comparatively high efficiency [64]. Moreover, the working fluid pentane is environmentally friendly. It has zero ozone depletion potential (ODP) and a global warming potential (GWP) that is more than 45 times lower compared to other working fluids like R245fa and R134a. In addition, pentane is not registered as a substance hazardous to human health or

the environment by the European Union (EU). Moreover, pentane has a high critical temperature and remains a liquid at ambient conditions, which minimizes handling cost [65].

The thermodynamic properties of pentane were acquired from a database program called NIST webbook (NIST standard Reference Database Number 69) [66]. The program was developed by the National Institute of Standards and Technology (NIST) and provides tables of the thermodynamic properties (for example density, enthalpy, entropy and saturation temperature) of most engineering working fluids.

3.3 Development of the model plant

The model power plant consists of an overhead hot water tank, cold water tank, cold water pump, working fluid reservoir, feed pump, evaporator, single stage impulse turbine and water cooled condenser as shown in the schematic diagram on Figure 3.1. Water was heated by an electric heater in the elevated hot water tank and flowed into the evaporator due to the potential difference between the evaporator and the hot water tank which had a pressure difference of 6.8 kPa. The cold water from the evaporator was collected in the cold water tank and pumped back to the overhead hot water tank where it was heated and circulated again.

The feed pump supplied pentane from the working fluid tank to the evaporator, where the working fluid was vaporized by heat transferred from the hot water. The high pressure vapor flowed into the turbine and expanded producing mechanical power. The low pressure vapor exhausted from the turbine was condensed by cooling water as it flowed through the condenser. The condensed working fluid was directed back into the reservoir and was pumped again into the evaporator and a new cycle began. Figure

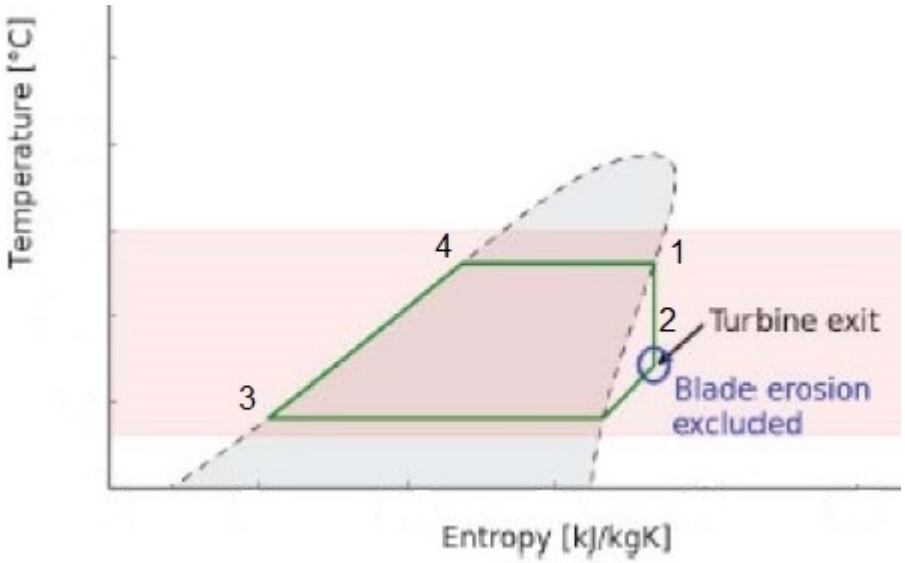

Figure 3.2: T-s diagram of the cycle [64]

3.2 is the T-s diagram of the cycle and shows that the pentane is a dry expansion type. The saturation curve is skewed to the right and shows expansion ended on the dry region on which no condensation happened in the turbine.

3.3.1 Design of the turbine

The turbine for the model Organic Rankine Cycle power plant was a radial flow single stage impulse turbine. This configuration was cost effective, simpler in construction and has better efficiency for low output power plants compared to a reaction turbine. Moreover, unlike in a reaction turbine, in which expansion takes place in fixed blades, in an impulse turbine velocity (or kinetic energy) of vapor increases in the nozzle and thus no expansion takes place in the moving blades and as such its pressure remains constant while passing over the blades.

The design equations and configurations of the turbine were adapted from the Steam Turbine Design document by Maurya A. [56]. Figure 3.3 shows the velocity diagram

at the inlet and exit of a single-stage impulse turbine. V_1 and V_2 are inlet and outlet

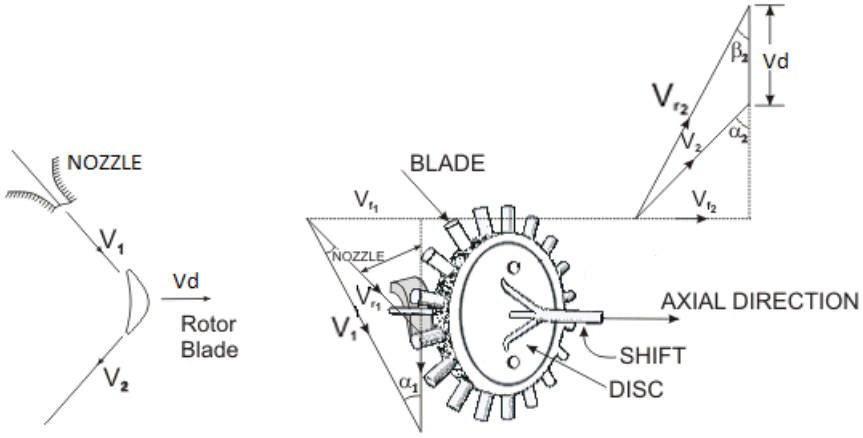

Figure 3.3: Velocity diagram of an Impulse Turbine [56]

absolute velocity respectively, V_{r1} and V_{r2} are the inlet and outlet relative velocities (velocity relative to the rotor blades.), V_d is the mean blade speed, α_1 is the nozzle angle, α_2 is the absolute fluid angle, β_1 and β_2 are the inlet and outlet blade angles. All angles are measured with respect to the tangential velocity (in the direction of V_d). The velocities V_{w1} and V_{w2} are tangential or whirl components of the absolute velocity at inlet and outlet, V_{f1} and V_{f2} are the axial components of velocity at inlet and outlet.

Tangential force on a blade (F_u):

$$F_u = \dot{m}\Delta V_w \tag{3.1}$$

Power developed ($\dot{W}$):

$$\dot{W} = \dot{m}V_d\Delta V_w \tag{3.2}$$

3.3.2 Fundamental nozzle energy relations

The flow of fluid in the nozzle was assumed to be one-dimensional, adiabatic, frictionless and steady flow. The change in fluid velocity and all thermodynamic properties occurs only in the direction of the flow. This means that the fluid velocity was assumed to remain constant at a mean value across the cross-section of the tubes. Hence the change in potential energy was neglected. Energy is conserved during flow of fluid through the nozzle as shown in Figure 3.4.

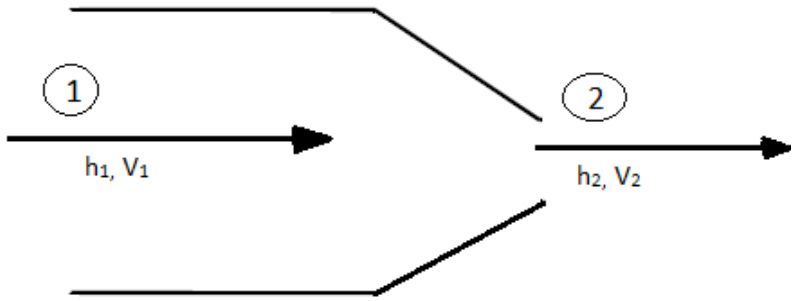

Figure 3.4: Flow through nozzle [56]

$$\frac{V_2^2 - V_1^2}{2} = h_1 - h_2 \tag{3.3}$$

Where h_1 - h_2 = Δh is the available energy.

3.3.3 Conversion of kinetic energy into work

The turbine blades were considered frictionless and turned the vapor through 180^o in which the absolute velocity of the vapor at the exit was zero. Hence maximum conversion of vapor kinetic energy into blade work was considered. The relation between the absolute velocity of the vapor entering the blade, V_1, and the blade speed, V_d, were

developed for a given vapor speed and used to design a nozzle.

$$V_1 = 2V_d \tag{3.4}$$

Actual nozzle angle

The nozzle angle values used in practice range from 12 to 20^0 . Larger angles are used usually at the low-pressure end of large turbines. Equation (3.4), corrected for a finite nozzle angle, α, becomes:

$$V_1 cos\alpha = 2V_d \tag{3.5}$$

3.3.4 Performance of the single stage turbine

Power developed by the turbine (expansion process 1-2, Figure 3.2 and 3.5) is given by:

$$\dot{W}_t = \dot{m}(h_2 - h_1) \tag{3.6}$$

Where h_1 is enthalpy at the inlet, h_2 is the actual enthalpy at the turbine exit and $\dot{W}_t$ is the actual power developed in the turbine. The quantities in Table 3.1 are the assumptions made in the design of the turbine to determine the performance of the turbine and inlet and exit conditions of the working fluid in the cycle.

Efficiency of the turbine (η_{turb}):

$$\eta_{turb} = \frac{h_2 - h_1}{h_{2s} - h_1} \tag{3.7}$$

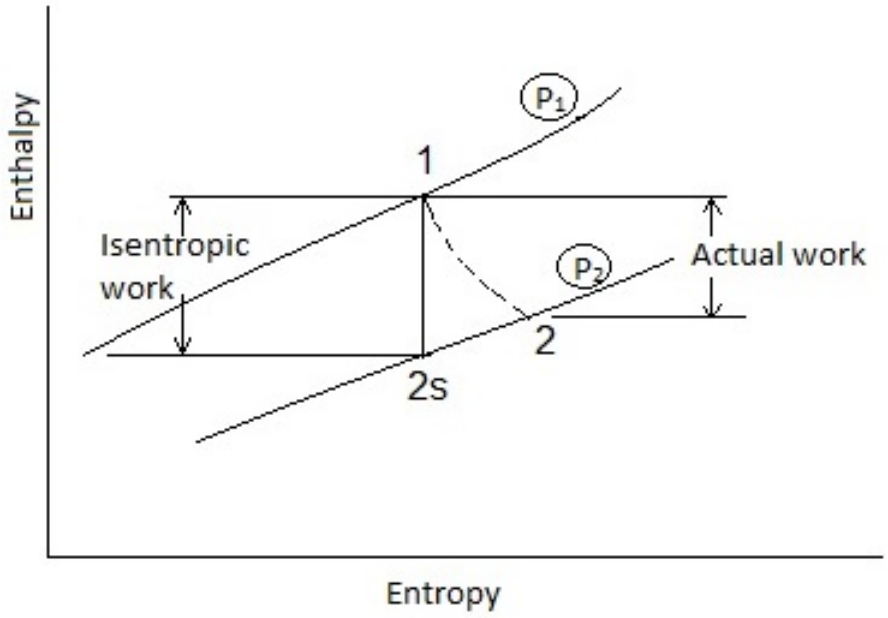

Figure 3.5: Turbine efficiency

Table 3.1: Assumptions made for the model power plant

S/No	Description	Value
1	Net power output	1 kJ/s
2	Turbine isentropic efficiency(η_{turb})	0.8
3	Turbine mechanical efficiency(η_{mech})	0.97
4	Boiler efficiency(η_b)	0.90
5	Generator efficiency(η_{gen})	0.70

Where h_{2s} is the enthalpy at isentropic turbine exit.

Ideal work of the turbine

$$\dot{w}_{ideal} = \frac{\dot{w}_{act}}{\eta_{turb}\eta_{mech}\eta_b\eta_{gen}} \tag{3.8}$$

Considering the assumptions in Table 3.1, the design process and thermodynamic analysis of the cycle were carried out. For ideal expansion in the turbine, the entropy of the fluid at the exit of the turbine, s_2, is the same as that of the fluid at the inlet to the turbine s_1 as shown in Figure 3.2 and 3.5. At a fixed turbine exit pressure and entropy s_1, the enthalpy of the fluid at state 2 (turbine exit) was obtained from the table of the thermodynamic properties of pentane. Thus the power output of the turbine ($\dot{W}_t$)

equals to:

$$\dot{W}_t = \dot{m}(h_{2s} - h_1) \tag{3.9}$$

The actual work(w_{act}) of the turbine (Figure 3.5) was determined using the following equations:

Table 3.2: Details of the turbine design

S/No	Quantity	Value	Inlet	Exit
1	Blade velocity(m/s)	5	-	-
2	Vapor tangential velocity(m/s)	-	11.7	-
3	Vapor relative velocity(m/s)	-	11	-
4	Vapor relative velocity(m/s)	-	6	-
5	Vapor axial velocity(m/d)	-	3.76	-
6	Vapor angle	-	32	32
7	Blade work	55	-	-
8	Blade efficiency	0.85	-	-
9	Turbine work(ideal)	43.42	-	-
10	Turbine work(actual)	23.38	-	-
11	Enthalpy	-	43.383	8.65
12	Vapor mass flow rate(kg/s)	0.085	-	-

$$W_{act} = \eta_{turb}\eta_{mech}\eta_{gen}W_{ideal} \tag{3.10}$$

The enthalpy at state 2 (h_2) was determined as follows:

$$h_2 = h_1 + (\eta_{turb}W_{ideal}) \tag{3.11}$$

Working fluid mass flow rate:

$$\dot{m}_{wf} = \dot{W}/W_{act} \tag{3.12}$$

The design details of the turbine are shown in Table 3.2 and the detailed evaluation of each property is given in the appendix A.

3.4 Heat exchangers design

Heat is transferred from one fluid to other in the heat exchanger. The heat transfer area, the overall heat transfer coefficient and the temperature difference were the main important factors considered [45]. For indirect heat transfer between two fluids, the shell and tube heat exchangers are more effective. In this study, a shell and tube type heat exchanger was selected for the evaporator of the model power plant due to the advantages of fairly simple geometry, can be fabricated from a wide range of materials and ease of cleaning.

Essentially, the shell and tube heat exchanger comprises a bundle of tubes whose ends were welded to a tube sheet within a cylindrical shell. The tube sheets also separate the shell side and tube side fluids in which one of the fluids was flowing inside the tube while the other circulated around the tubes. Baffles were provided in the shell side to support the tubes, maintain uniform spacing between the tubes and direct the flow of the working fluid across the tubes to enhance heat transfer.

The design of the heat exchangers involved establishing the right flow configuration. Parallel flow and counter flow are the main flow patterns in shell tube heat exchangers. The counter flow configuration was the preferred flow direction in liquid to liquid heat exchangers. This flow configuration has a higher temperature difference that drives the heat transfer within the heat exchanger which in turn results in a smaller heat transfer area [53]. Moreover, the counter flow configuration is the most effective design when the desired outlet temperature of the cold fluid is between the inlet and outlet temperatures of the hot fluid [67].

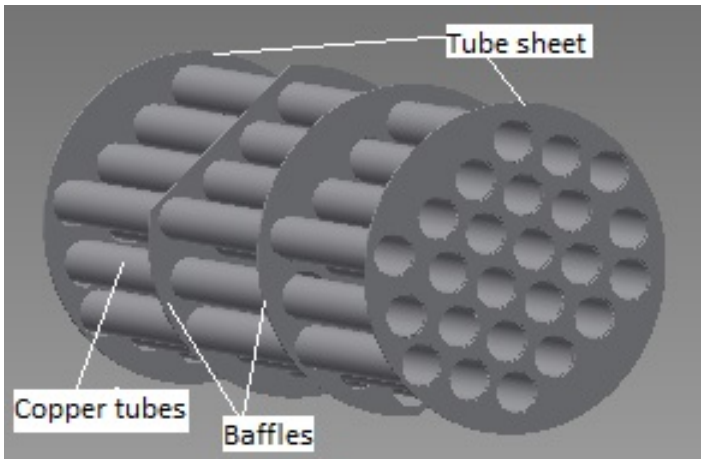

Figure 3.6: The main components of the evaporator

3.4.1 Heat exchanger sizing and rating

The evaporator is the main component of the model Organic Rankine Cycle power plant. It receives heat energy from the hot water to vaporize the organic working fluid (pentane). The design of an evaporator was achieved through a fixed tube counter flow shell and tube type heat exchanger where the hot water flows in the tube side and working fluid (n-pentane) vaporizes in the shell side. This type of fluid pattern allowed the fouling fluid to flow through the tubes (easier to clean) and the organic working fluid (pentane), which has lower mass flow rate, was flowing through the shell. The heat exchanger was designed with a shell diameter of 150mm and a tube length within the shell of 550mm. This sizing established the optimum distribution of the copper tubes within the heat exchanger shell. Figure 3.6 shows the main components of a shell tube heat exchanger. The heat transferred from one fluid to another is proportional to the mass flow rate and temperature difference.

$$\dot{Q}_{1-2} = \dot{m} c_p \Delta T \tag{3.13}$$

Where $\dot{m}$ is the mass flow rate of the fluid, ΔT is the temperature difference between inlet and exit and c_p is the specific heat capacity at constant pressure.

3.4.2 Heat exchanger tube sheets

The tube sheet pitch represents the distance between the centers of the two adjacent tube hole. The optimum pitch of 1.25 times the outside tube diameter was used to provide uniform distribution of tubes. A 30^o triangular pitch tube configuration (Figure 3.6) was applied to provide higher heat transfer and compactness due to greatest tube density. The copper tubes were inserted into the holes in the tube sheets and firmly brazed to the tube sheet. The tube sheet was welded to the main shell to provide the maximum heat transfer area for given shell and tube diameters.

3.4.3 Heat exchanger baffles

Two baffles were provided as shown in Figure 3.6 with a baffle pitch of 150 mm. The optimum baffle pitch (spacing between segmental baffles) and the baffle cut were used to determine the cross flow velocity and hence the rate of heat transfer and minimize pressure drop. A baffle spacing of 0.2 to 1 times of the inside shell diameter has been most practically used. A baffle cut of 20 to 25% provides a good heat transfer with reasonable pressure drop [68]. In this particular heat exchanger, a 20% baffle cut was used as it supported a greater number of tubes with better space for fluid to flow across the tubes.

3.4.4 Evaporator sizing and rating

Heat energy is transferred from the hot water to the organic working fluid (n-pentane) within the evaporator. In the design of heat exchangers, it is reasonable to assume a constant value of the overall heat transfer coefficient (U). The log mean temperature difference (LMTD) is useful for sizing and rating of a heat exchanger of known mass flow rate and range of temperature difference between the inlet and outlet of fluid streams as shown in Table 3.3. The following equations were used in relating the heat transfer surface area through which heat flow occurs under the driving force of temperature difference, the amount of heat transferred and the overall heat transfer coefficient.

Heat transferred in the process ($\dot{Q}$) was related to the mean temperature difference

Table 3.3: Flow conditions of the fluid streams in the heat exchanger

S/No	Description	Tube side	Shell side
1	Mass flow rate (kg/s)	0.1	0.12
2	Inlet Temperature (^{o}C)	54	25
3	Outlet Temperature (^{o}C)	36	51

and the overall heat transfer coefficient (U) using the equation 3.14:

$$\dot{Q} = UA\Delta T_{LMTD} \tag{3.14}$$

Where A is heat transfer surface area and ΔT_{LMTD} is the log mean temperature difference. The log mean temperature difference of a counter flow heat exchanger is given by:

$$\Delta T_{LMTD} = \frac{\Delta T_2 - \Delta T_1}{\ln(\frac{\Delta T_2}{\Delta T_1})} \tag{3.15}$$

Where, ΔT_1 and ΔT_2 represent the temperature differences at the inlet and exit of the heat exchanger respectively as indicated in Figure 3.7. The parameters in Table 3.4 are the assumption made in the inlet and exit conditions to determine the size and rate

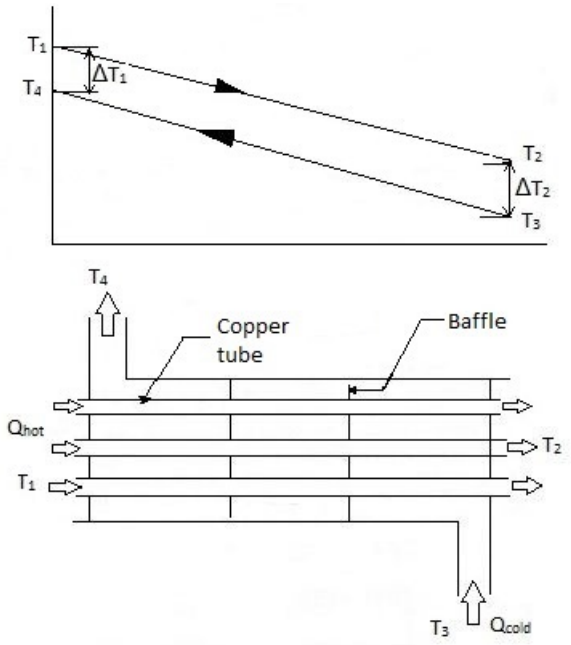

Figure 3.7: Counter flow heat transfer in the shell and tube heat exchanger

of the heat exchanger.

The log mean temperature difference for counter flow shell tube heat exchanger was

Table 3.4: Assumptions in the design of the evaporator

S/No	**Property**	**Value**
1	Heat transfer coeff.(U)(W/m^2.^{o}C)	3000
2	Hot water flow rate ($\dot{m}_w$)(kg/sec)	0.1
3	Pentane flow rate($\dot{m}_{wf}$)(kg/sec)	0.12
4	Hot water inlet temp(T$_{hi}$)(^{o}C)	54
5	Hot water outlet temp(T$_{ho}$)(^{o}C)	36
6	Pentane inlet temp(T$_{ci}$)(^{o}C)	25

evaluated using the following relations and Figure 3.7: Where D is the diameter of copper tube.

$$\Delta T_{LMTD} = \frac{(T_1 - T_4) - (T_2 - T_3)}{\ln[\frac{(T_1 - T_4)}{(T_2 - T_3)}]} \tag{3.16}$$

Heat exchanger surface area:

$$A_s = \frac{\dot{Q}_{1-2}}{U \Delta T_{LMTD}} \tag{3.17}$$

Total length of the copper tube:

$$L = \frac{A_s}{\pi D} \tag{3.18}$$

Number of copper tubes in the shell (Tube-count):

Table 3.5: Dimensions and parameters of the evaporator

S/No	Description	Tube side	Shell side
1	Fluid type	hot water	pentane
2	Number of tubes	33	-
3	Total tube length(m)	13.1	-
4	Tubes diameter (DO/DI)(mm)	12.7/10.9	150
5	Heat transfer area(m^2)	0.41	-
6	Number of pass	1	-
7	Tube configuration	30^o triangular	-
8	Tube pitch(mm)	16	-
9	Material	Copper	galvanized steel

Tube count represents the number of copper tubes in the shell. The length of tube in the shell is 40 cm, therfore the number of tubes inside the shell was determined as:

$$N_{tb} = \frac{A_s}{\pi D l} \tag{3.19}$$

where N_{tb} is the number of tubes in the shell and l is the length of copper single tube inside the shell .

The details of the design and core dimensions of the evaporator are summarized in Table 3.5. The details of the evaluation of the size of the evaporator is given in appendix B.

3.4.5 Condenser sizing and rating

Research done by Brasz *et al.* [69] showed that the water cooled condensation in Organic Rankine Cycle results in lower condensing temperatures and therefore higher cycle efficiency than can be achieved with typical air cooled condenser under same conditions.

Table 3.6: Assumptions in the design of the condenser

S/No	Property	Value
1	Heat transfer coeff.(U)(W/m^2.^{o}C)	16000
2	Cooling water flow rate ($\dot{m}_w$)(kg/sec)	0.3
3	Pentane flow rate($\dot{m}_{wf}$)(kg/sec)	0.12
4	Pentane inlet temp(T_3)(^{o}C)	51
5	Pentane outlet temp(T_4)(^{o}C)	25
6	Cooling water inlet temp(T_{ci})(^{o}C)	20
7	(C_p)(kJ/kg.K) at 1 bar and 55.0^o	1.8337
8	(C_p)(kJ/kg.K) at 1 bar and 36.0^o	20
9	(C_p) average (kJ/kg.K)	1.7985

The condenser of the model power plant was a water cooled fixed tube, counter flow shell and tube heat exchanger. The flow configuration of the heat exchanger was in such a way that the cooling water flowed in the tube side whereas the working fluid (n-pentane) flowed in the shell side.

The condenser was designed such that the shell diameter was 150 mm and tube length was 400 mm. The sizing was selected to determine the optimum distribution of the copper tubes within the heat exchanger shell. The tube material was of good thermal conductance hence the thickness of the tube was assumed negligible. The size of the condenser was evaluated using equations 3.13 to 3.19 and the design details and dimensions are summarized in Table 3.7. The detailed evaluation of the condenser is given in appendix B.

3.5 Fabrication of the main components of the model plant

The design of the main components of the model heat recovery Organic Rankine Cycle power plant considered the availability of the materials and achievable fabrication methods. The two heat exchangers (evaporator and condenser), water heating tank and single stage impulse turbine were fabricated in accordance to the design.

Table 3.7: Dimensions and parameters of the condenser

S/No	Description	Tube side	Shell side
1	Fluid type	pentane	cooling water
2	Number of tubes	21	-
3	Total tube length(m)	8.4	-
4	Tubes diameter (DO/DI)(mm)	12.7/10.9	150
5	Heat transfer area(m^2)	0.2634	-
6	Number of pass	1	-
7	Tube configuration	30^o triangular	-
8	Tube pitch(mm)	16	-
9	Material	Copper	galvanized steel

3.5.1 Fabrication of the turbine

The turbine of the model power plant was fabricated through casting. Aluminum alloy was used for casting all turbine parts due to its sufficient mechanical strength and relatively light weight that makes it convenient for the mini turbine. Moreover, the ease of casting process and machinability are also the main advantages of aluminum alloy.

The pattern, which is a full size model of the part or component to be cast, was prepared from wood in an identical shape but slightly greater size to account for the shrinkage during casting and machining allowance in the final casting. Moreover, all sharp corners were filleted and the vertical surfaces were tapered on each pattern to facilitate easy removal of the pattern from the mold and reduce damage of edges in the mold. The summary of the casting procedure followed for each turbine component is summarized in appendix A.

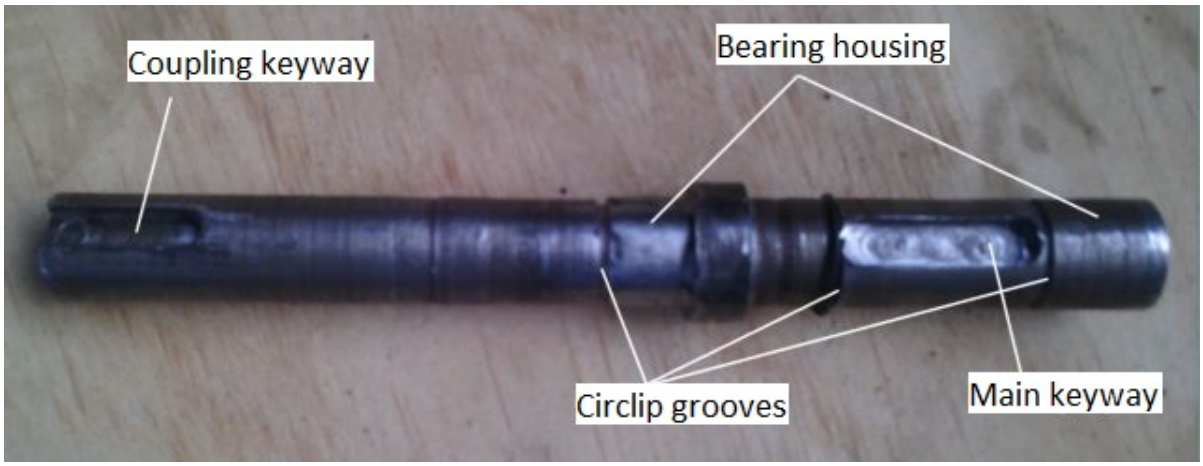

Figure 3.8: The shaft of the turbine

3.5.2 Fabrication of the turbine shaft

The turbine shaft is the output device used to drive the model generator. The turbine shaft was prepared by turning a 25 mm steel rod. Two keyway grooves were machined along the axis of the cylindrical surface of shaft. The first keyway groove was machined, into which a key was fitted to provide a positive method of locating and driving the turbine rotor on the shaft. The second keyway was prepared on the other end of the shaft to provide positive drive for the model generator. Two 2 mm by 1 mm grooves were also machined for the circlips on each end of the main keyway to avoid sliding of the rotor on the shaft. Figure 3.8 shows the position of each groove on the shaft.

3.5.3 Fabrication of the heat exchangers

The shell of the heat exchanger was constructed by rolling a plate of 2 mm thick galvanized steel. The plate was cut to a rectangular shape of size 471 mm by 750 mm and four holes were drilled for the inlet and outlet of the two fluids before rolling the plate. After rolling, a shell of 150 mm diameter by 750 mm length was obtained. The copper tubes were held at the ends by means of galvanized iron sheets as shown in Figure 3.9.

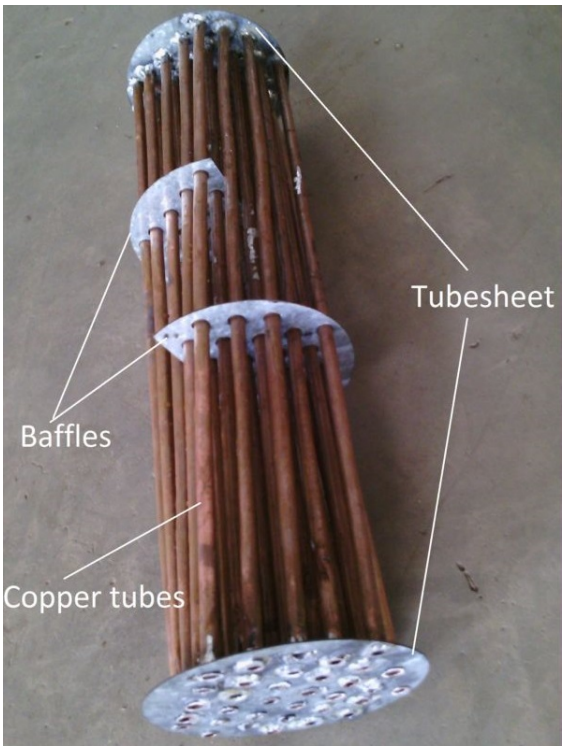

Figure 3.9: The shell and tube heat exchanger

Two baffles were also provided at a baffle pitch of 150 mm. The optimum baffle pitch (spacing between segmental baffles) and the baffle cut were used to determine the cross flow velocity and hence the rate of heat transfer and to minimize pressure drop. Copper tubes were cut at a length of 40 cm and each tube was brazed using gas welding to the hole provided on the tube sheet to produce a tube bundle (Figure 3.9). The tube bundle was then inserted to the shell and the two tube sheets were spot welded using arc welding and then brazed using gas welding to provide leak proof joints.

3.5.4 Fabrication of the hot water tank

The cylindrical hot water tank was constructed by rolling a plate of galvanized steel of 2 mm thickness. The plate was cut to a rectangular shape of size 1260 mm by 570 mm.

After rolling, a cylindrical tank of 400 mm diameter by 750 mm height was obtained. A 3kw electric water heater was fixed to cylinder at the height of 100 mm from the base. The electric heater had a knob for varying the resistance and hence the temperature range from minimum to maximum.

3.5.5 Turbine assembly

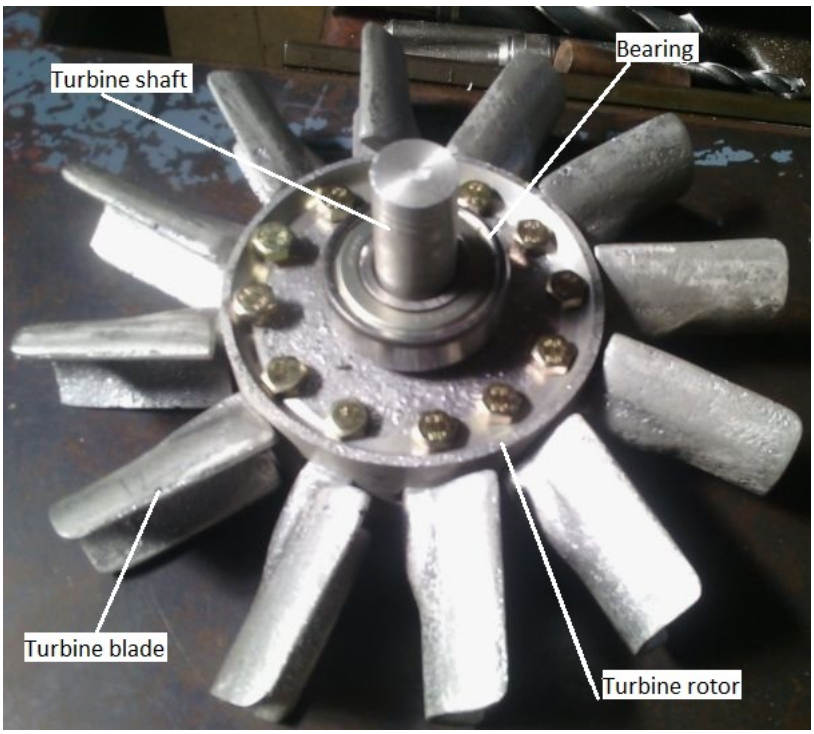

Figure 3.10: The turbine blade and rotor assembly

All the blades were placed on the seats provided on the turbine rotor and glued together before drilling. Glue fastening was done as temporary fastening to avoid vibration and misalignment of the blades while drilling together with the rotor. The rotor and blades were fastened by a 6 mm bolts as shown in Figure 3.10.

The turbine runner (the rotor and blades) were then assembled to the shaft using

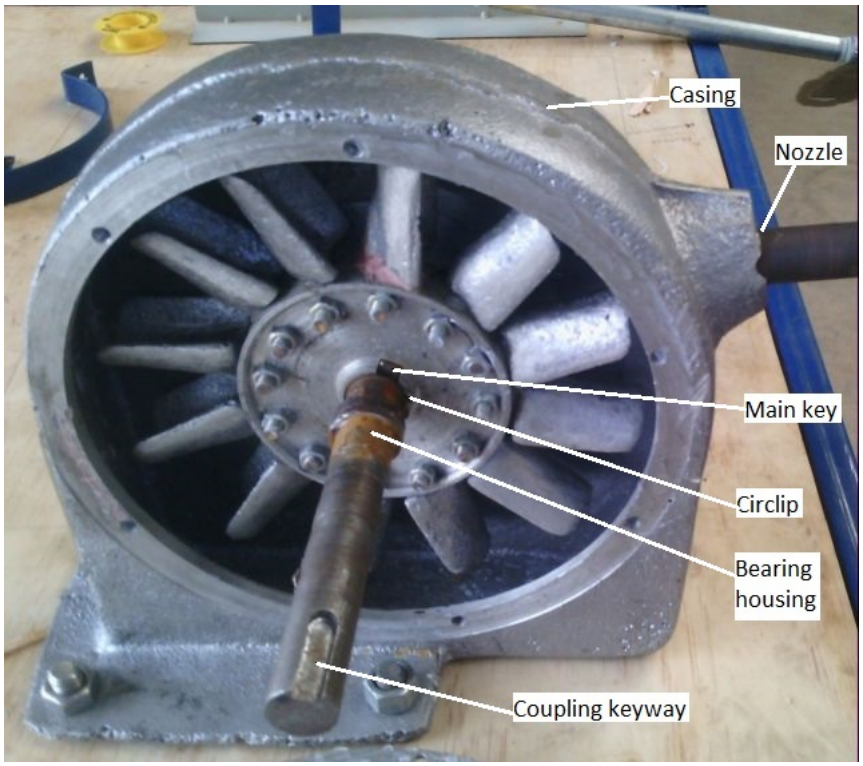

Figure 3.11: The turbine components assembly

keyways and circlips were placed at the two ends of the key to prevent sliding of the rotor over the shaft as shown in Figure 3.11. The runner, shaft, bearings, gaskets, and the casing were assembled together into a turbine. Two single row radial deep groove ball bearings, (NACHI 6204ZE type) which are of stainless steel type were pressed on the shaft and inserted into the bearing holes in the casing.

3.5.6 Assembling of the ORC model power plant

The components of the model power plant were fabricated as per the design specifications and assembled together as shown in Figure 3.12.

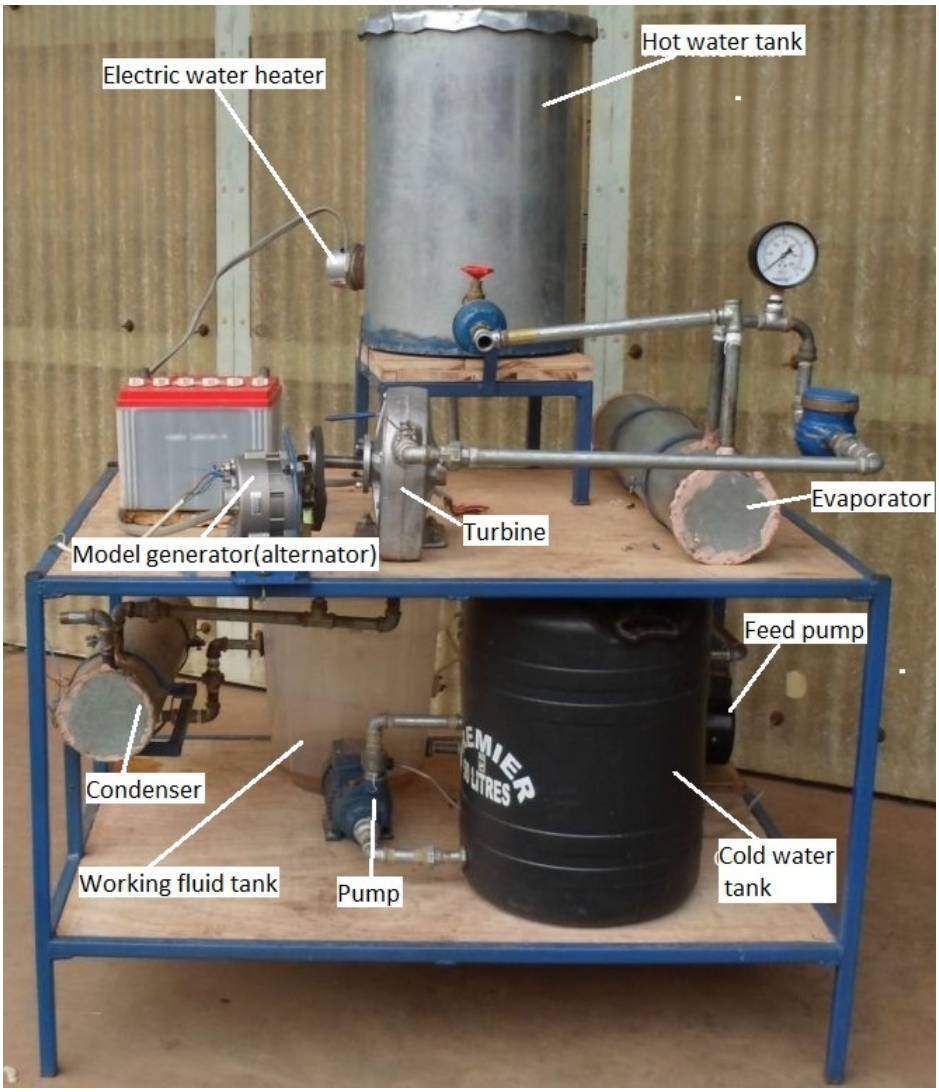

Figure 3.12: The Organic Rankine Cycle model power plant.

3.6 Performance test of the components of the plant

The main components of the model waste heat recovery system for geothermal brine based on an Organic Rankine Cycle (ORC) were designed and fabricated. The design and optimization of each component determines the efficiency of the model power plant. However, working fluid leakage and thermal losses are the main challenges of ORC systems. An experimental setup was built to test the performance of the main components (evaporator, condenser and turbine) of the model ORC system at different

operating conditions. The system performance was conducted using an environmentally friendly working fluid (pentane) and the performance parameters of the heat exchangers were evaluated.

3.6.1 Turbine performance test

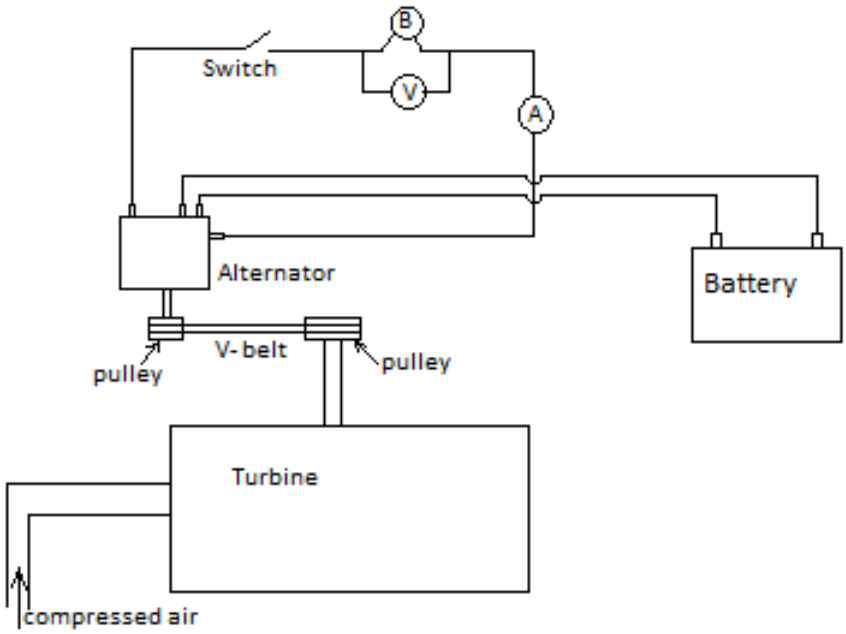

Figure 3.13: Schematic of turbine performance test set up

The schematic diagram of the experimental setup for the performance test of the impulse turbine is shown in Figure 3.13, which Figure 3.14 shows the pictorial representation. Air from the compressor to the turbine was passed through a 25 m hose. The air entered the pressure regulator before it flowed into the turbine blades through the nozzle in the casing, expanded in the turbine and then left the casing. The maximum pressure of the air was 8 bars but the air tank was used for short durations as the turbine was an open system.

The 60 W car alternator was used as the generator model, it was connected to the

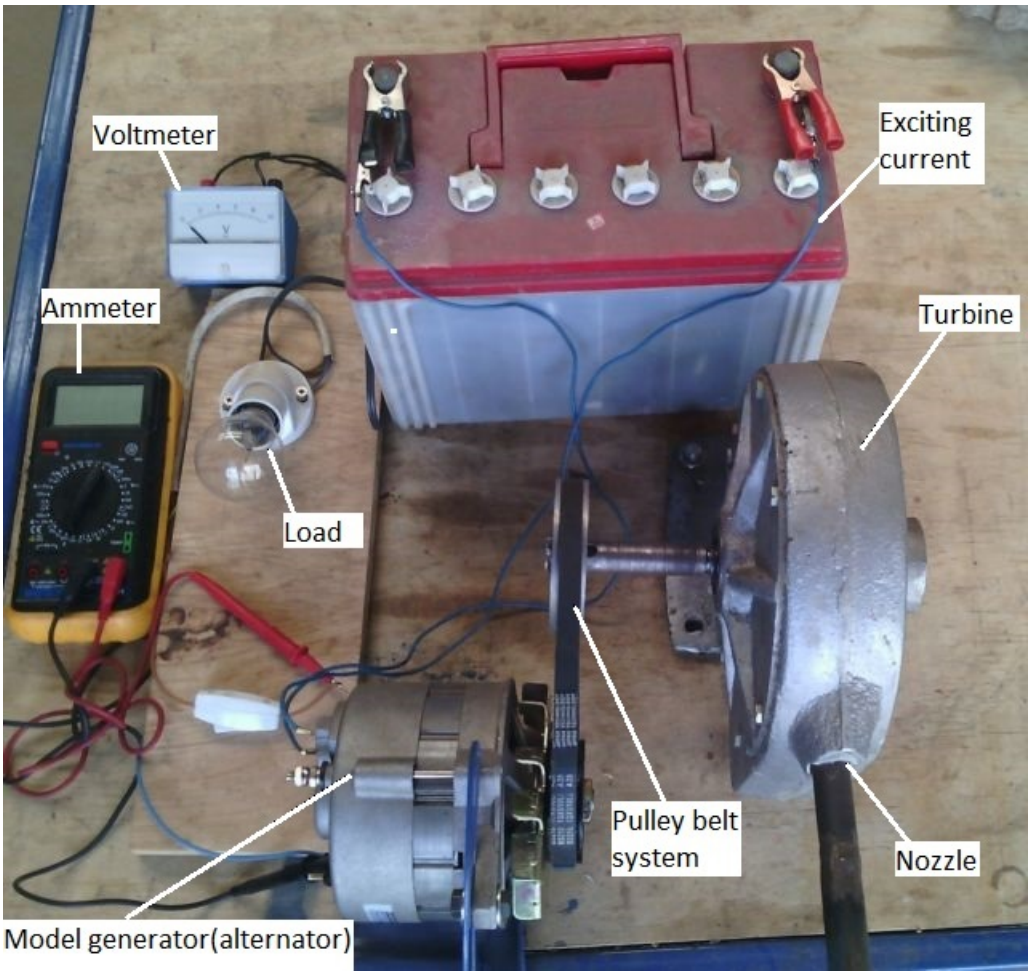

Figure 3.14: Photograph of the turbine performance test set up

turbine using a pulley and belt system to convert the mechanical energy of turbine shaft to electrical energy. The alternator is an electromechanical device which uses a rotating field winding excited with direct current, and a stationary (stator) winding that produces alternating current. It has a built-in current rectifier circuit to generate DC output. A 12 V battery was connected to the alternator to supply exciting current and a load of 18 W DC bulb was connected in parallel to indicate the electrical power generated and the outputs were tested using the setup shown in Figure 3.13 and 3.14.

Measurement procedure:

A set of ten experiments were conducted by varying the inlet pressure at an increment

of 0.5 bar. Two shaft speed measurements were taken for each inlet pressure, when the alternator exciting current was switched off (turbine no-load case) and with the exciting current switched on (turbine fully loaded). The voltage was measured across the bulb using a voltmeter and an ammeter was connected in series with the bulb to measure the current in the circuit. The experiment was conducted successfully and the measurements were recorded.

Evaluation of the power output:

The outputs of the model generator were directly measured in terms of voltage (V) and current (I). The power output ($\dot{W}$) was evaluated using the relation below:

$$\dot{W} = VI \tag{3.20}$$

3.6.2 Heat exchangers leakage test

It is important to ensure there is no leakage of fluids in the evaporator and condenser at the operating temperature and pressure before carrying out a performance test. The heat exchangers were tested for leakages using water both for the shell side and tube side. Water pumped at a pressure of 2.5 bar was used for this test. Any leaking sections (particularly at the welded joints) were sealed using a sealing material known as stag. Stag is a semi liquid joining paste commonly used for galvanized joints in pipes. It has a working temperature range of 0 to 60^{o}C. Moreover, it is water and organic fluid proof and also lead-free joining compound. It was applied to the evaporator and condenser since it is non-poisonous and does not react with pentane and water.

3.6.3 Performance test of evaporator and condenser

The performance test unit consists of an overhead hot water tank, evaporator, condenser, working fluid tank and feed pump. A schematic sketch showing valves, pressure gauges, flow meters and the location of temperature sensors is given in Figure 3.15. The hot water, produced by an electric heater in the hot water tank, flowed due to the potential difference through the evaporator in the tube side. Hot water flow rate was controlled by opening the flow valve HV1.

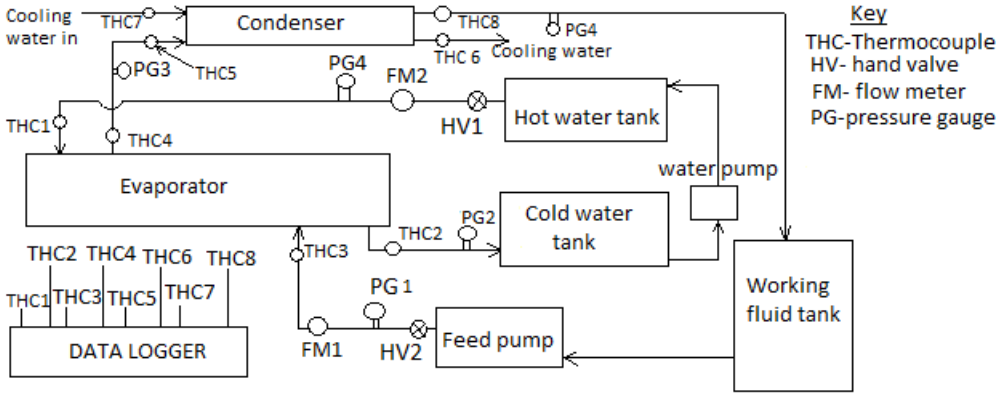

Figure 3.15: Schematic sketch of the evaporator and condenser performance test experiment.

The working fluid (n-pentane) was supplied by the feed pump to the evaporator through the flow meter FM1 and the flow rate was controlled by the flow valve HV2. Pentane was vaporized on the shell side in a counter flow to that of hot water. The evaporator and condenser were connected so that the vaporized working fluid (n-pentane) flowed directly to condenser. The heat transferred from hot water into the working fluid was rejected in the condenser as it flowed on the shell side while the cooling water flowed in the tube side. The condensed pentane flowed back to the working fluid tank.

The duration of one test was set to two minutes. A set of eight thermocouples were provided to record pertinent temperatures at the inlet and exit of each fluid as shown

in Figure 3.15. All the thermocouples were connected to a data logger called TDS-530. The temperature indicators on the data logger displayed the inlet temperature of hot water to evaporator (T_1), the exit temperature of cold water from the evaporator (T_2), the inlet temperature of the working fluid to the evaporator (T_3), the working fluid exit temperature from the evaporator (T_4), the inlet temperature of the working fluid to condenser (T_5) and the exit temperature of the working fluid from condenser (T_6), the inlet temperature of the cooling water to the condenser (T_7), and the outlet temperature of the water from the condenser (T_8).

Measurement procedure:

A set of five measurements were taken by varying the hot water mass flow rates. The evaporator and condenser were connected so that the vaporized working fluid (n-pentane) flowed directly to the condenser. The heat transferred from the hot water into the working fluid was rejected in the condenser and the condensed pentane flowed back to the working fluid tank. The inlet and exit temperatures and pressures of each heat exchanger were recorded for every test run.

Evaluation of the thermal parameters:

The following relations were applied to evaluate the performance parameter (heat duty, overall heat transfer coefficient and pressure drop) within the heat exchangers. The log mean temperature difference (LMTD) method was used since the inlet and outlet temperatures of both the hot water and the working fluid were known.

1. Evaporator heat duty:

$$\dot{Q}_{eva} = \dot{m} c_p \Delta T \tag{3.21}$$

where $\dot{m}$ is the mass flow rate of pentane, c_p is the specific heat at constant pressure and ΔT is the temperature change between inlet and exit of the evaporator.

2. Evaporator overall heat transfer coefficient:

$$U_{eva} = \frac{\dot{Q}_{eva}}{AdtT_{LMTD}} \tag{3.22}$$

where A is the effective heat transfer area of the evaporator and T_{LMTD} is the log mean temperature difference between inlet and exit of the evaporator.

3. Condenser heat duty:

$$\dot{Q}_{con} = \dot{m}c_p\Delta T \tag{3.23}$$

where $\dot{m}$ is the mass flow rate of pentane, c_p is the specific heat at constant pressure and ΔT is the temperature change between inlet and exit of the condenser.

4. Condenser overall heat transfer coefficient:

$$U_{con} = \frac{\dot{Q}_{con}}{AdtT_{LMTD}} \tag{3.24}$$

where A is effective condenser heat transfer area and T_{LMTD} is the log mean temperature difference between inlet and exit of the condenser.

5. Pressure drop of hot water:

$$\Delta P_w = P_o - P_i \tag{3.25}$$

6. Pressure drop of pentane:

$$\Delta P_p = P_i - P_o \tag{3.26}$$

7. Hot water temperature range:

$$\Delta T_w = T_{wi} - T_{wo} \tag{3.27}$$

8. Pentane Temperature range:

$$\Delta T_p = T_{pi} - T_{po} \tag{3.28}$$

9. Log mean temperature difference T_{LMTD} for counter flow heat exchanger:

$$T_{LMTD} = \frac{(T_{wi} - T_{po}) - (T_{wo} - T_{pi})}{ln(\frac{(T_{wi} - T_{po}}{T_{wo} - T_{pi}})} \tag{3.29}$$

Where:

T_{wi} is the hot water inlet temperature, T_{wo} is the hot water outlet temperature, T_{pi} is the pentane inlet temperature, and T_{po} is pentane outlet temperature.

Experimental procedures:

The overhead hot water tank was filled with water. The electric water heater built in the hot water tank was switched on and temperature was set to 54^{o}C. The inlet valve HV1 was opened and the hot water was allowed into the tube side of the evaporator. The feed pump was switched on and the working fluid (n-pentane) allowed to flow into the shell side of the heat exchanger (evaporator). The steady state measurements were attained in 36 minutes and all the four temperatures and flow rates of hot water and working fluid were recorded.

The performance tests of the evaporator, condenser and turbine were successfully conducted and the measurements were taken at the steady state conditions. Each test was repeated to ensure the accuracy of the results.

CHAPTER FOUR

4.0 RESULTS AND DISCUSSION

4.1 Performance test of the evaporator

The performance assessment test of the evaporator was conducted using two fluids, the hot water and the organic working fluid (n-pentane). Three parameters were studied to understand the performance of the heat exchanger: The heat transferred, overall heat transfer coefficient, and tube side and shell side pressure drop within the shell tube heat exchanger having hot water in the tube side and working fluid (n-pentane) in the shell side in counter flow configuration. Five performance tests were conducted at different hot water mass flow rates.

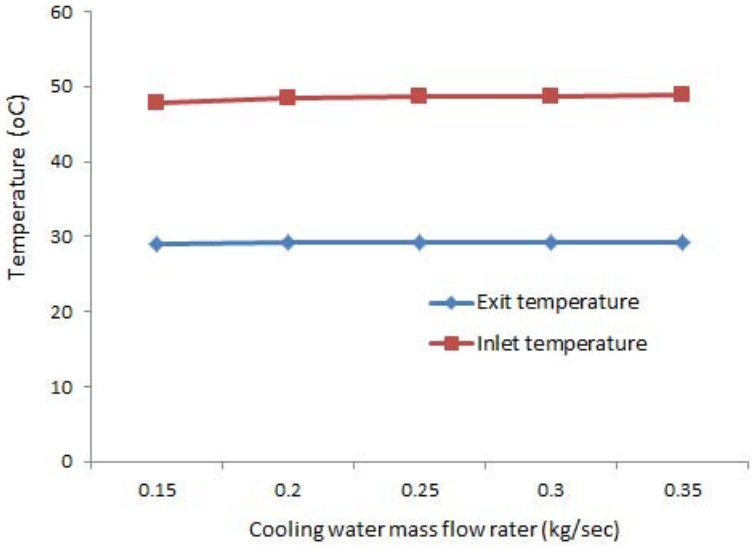

Figure 4.1: Variation of the inlet and exit temperature of pentane with increase in hot water flow rate in the evaporator

The variation of the temperatures at inlet and exit from the evaporator during the performance test is depicted in Figure 4.1. The changes of the inlet temperature of the working fluid (pentane) were insignificant since the working fluid was saturated liquid

from the condenser. However, the exit temperature of pentane was raised by more than 2%. This temperature rise attributes to the more heat transfered due to increase in mass flow rate of hot water by 50%.

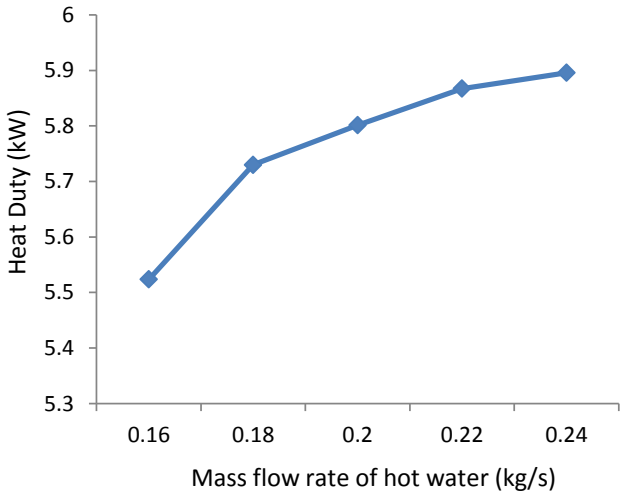

Figure 4.2: Variation of heat duty with increase in hot water flow rate in the evaporator

Furthermore, the increase in the mass flow rate of hot water resulted in variation on the amount of heat transferred (heat duty) as shown in Figure 4.2. It was observed that a 50% rise in hot water mass flow rate resulted to an increase in heat transfer by more than 6%. This is because increase in the hot water mass flow rate increases overall heat transfer coefficient. The performance of the evaporator was evaluated in terms of heat lost by hot water and heat gained by the working fluid and it was found that the average overall heat transfer efficiency of the evaporator was 61% which implies there was effective heat transfer between the two interacting fluids.

Similarly, the variation of overall heat transfer coefficient against the hot water mass flow rate is shown in Figure 4.3. The increase of the hot water mass flow rate by 50% caused a rise in the overall heat transfer coefficient of the heat exchanger by more than 17%. This proves that the heat energy transferred was varying positively with the mass flow rate of hot water. Considering that the specific heat capacity remains constant

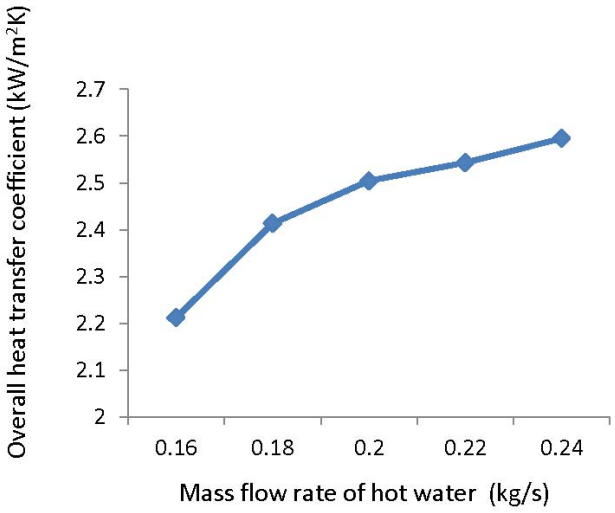

Figure 4.3: Variation of overall heat transfer coefficient with increase in hot water flow rate in the evaporator

through the heat exchanger, the hot water outlet temperature should decrease due to the heat loss. This complies with the law of energy conservation. Therefore as the flow rate of the hot water was increased, the tube side overall heat transfer coefficient also increased since the heat transfer area was constant.

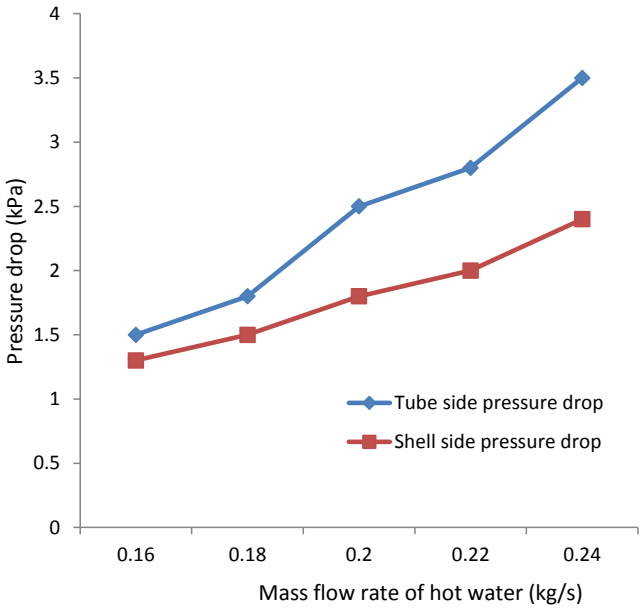

Figure 4.4: Variation of pressure drop with flow rate of hot water in the evaporator

Figure 4.4 reveals the variation of tube side and shell side pressure drop values with different values of hot water mass flow rate. It was observed that the pressure drop increased by more than twice in the tube side and in the shell side pressure drop increased by about 85% with the variation of hot water flow rate in the heat exchanger. Shell and tube heat exchangers generally experience pressure drop mainly due to friction, change in thermodynamic properties like viscosity and density through the heat exchanger as a result of heating or cooling, acceleration and deceleration of fluid with change in flow cross section. This pressure drop may increase the pumping power and may affect the service time of structural components of the heat exchanger. However, compared to the rate of change of the heat transferred, the rate of increase in pressure drop is reasonable.

4.2 Performance test of the condenser

The hot working fluid (pentane) flowing from the evaporator was condensed in the shell side of the condenser. Cooling water was supplied from a tap at different flow rates. Three parameters were studied to establish the performance of the heat exchanger: The heat transferred, overall heat transfer coefficient, and pressure drop within the shell and tube heat exchanger. Five experiments were conducted at different cooling water mass flow rates.

The change of the temperatures at inlet and exit from the condenser during the performance test is shown in Figure 4.5. It was observed that the average temperature of the working fluid at the inlet was 47.5^{o}C. However, the exit temperature from the condenser decreased by 1.4% with increase in cooling water mass flow rate by more than two times. This is due to the greater amount of heat rejected from the working fluid as the cooling water was increased.

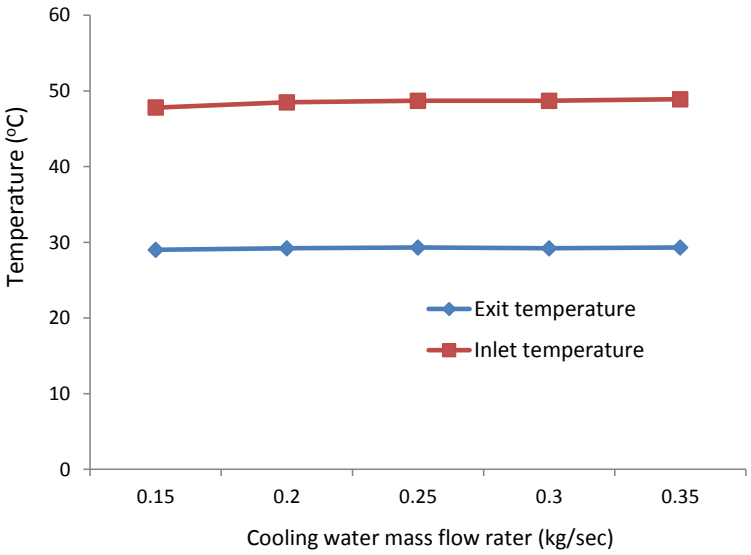

Figure 4.5: Variation of the inlet and exit temperature of pentane with increase in cooling water flow rate in the condenser

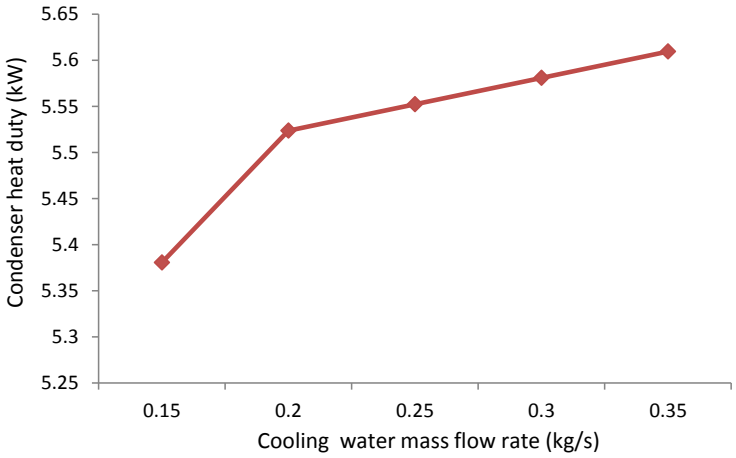

Figure 4.6: Variation of heat duty with increase in cooling water mass flow rate

In a similar way to the evaporator, change in the cooling water mass flow rate resulted in variation in the heat transferred (heat duty of the condenser) as shown in Figure 4.6. The results of the test revealed that heat transferred during the process was increased by 4.26% with a rise in cooling water mass flow rate by more than twice. This validates that heat transfer is directly related to the cooling water mass flow rate see Eq 3.13. It was observed that between the first and second test, the heat transferred (cooling

capacity) increased sharply. This shows that the condenser performs at lower efficiency for low cooling water mass flow rates.

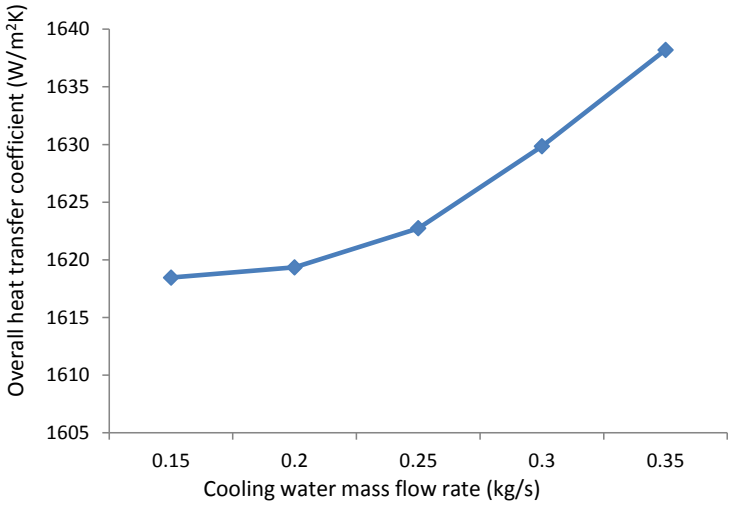

Figure 4.7: Variation of overall heat transfer coefficient with increase in cooling water mass flow rate in the condenser

Furthermore, changes in the mass flow rate of cooling water resulted in variation in the overall heat transfer coefficient of the heat exchanger as shown in Figure 4.7. The curve shows that an increase of cooling water mass flow rate by more than twice raised the overall heat transfer coefficient of the heat exchanger by 1.21%. This corroborates the relation between heat transfer and the overall heat transfer coefficient (Eq 3.14). Since the specific heat capacity of the working fluid remains almost constant, the outlet temperature of the working fluid should decrease and the cooling water outlet temperature should increase due to heat transfer from the hot fluid to the cold fluid and hence as the flow rate of the cooling water was increased, the overall heat transfer coefficient also increased.

Figure 4.8 shows the variation of tube side and shell side pressure drop values with increase in cooling water mass flow rate. It was observed that the tube side pressure

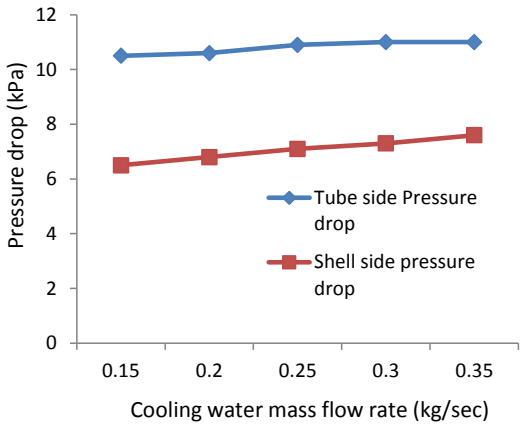

Figure 4.8: Variation of pressure drop with flow rate of cooling water in the condenser

drop was increased by nearly 5% in the tube side and the shell side pressure drop was raised by about 17% as the mass flow rate of the cooling water was raised by more than twice. In shell and tube heat exchangers (especially condensers) pressure drop is a common experience mainly due to phase change (condensation) and formation of re-circulation zones near the baffles. Moreover, other causes of pressure loss are change in thermodynamic properties like viscosity and density through the heat exchanger as a result of heating or cooling.

4.3 Performance test of the impulse turbine

The performance test of the single stage impulse turbine was carried out using compressed air. The shaft of the turbine was coupled to a car alternator as shown in Figure 3.13 and 3.14. The results of the performance tests revealed that the rotational shaft speed of the turbine increased very fast at the first four air feed pressures,i.e between 0 and 2 bars, and in the remaining six air feed pressures the change in speed of the shaft was gradual. The variation of shaft speed against the inlet pressure is shown in Figure 4.9. The performance of the turbine can be analyzed by dividing the curve into three

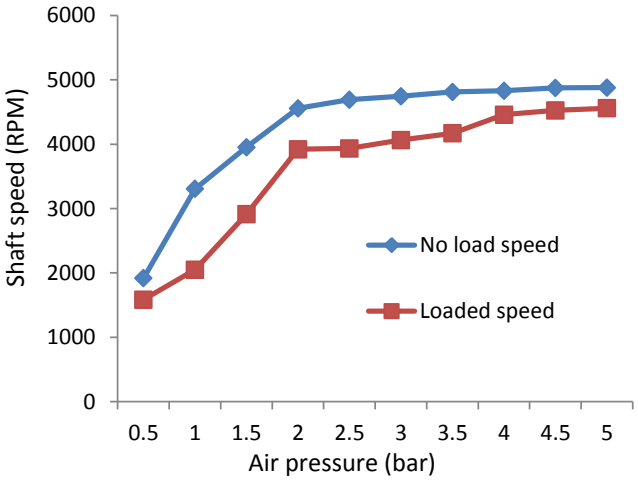

Figure 4.9: Turbine shaft rotational speed vs inlet air pressure

sections according to the slope of the curve. For the case in which the exciting current of the alternator was switched off (turbine no load case), in the first two performance tests doubling of the inlet pressure caused the speed of the shaft to increase by more than 72%. In the next two tests (test 3 and 4), doubling of the inlet pressure raised the rotational speed of the shaft by about 38%. In the last six tests (test5 to test 10), the rise of the inlet pressure by more than twice caused an increase of the shaft speed of the turbine by only 7.2%. The results of the test revealed that the turbine performance was improved with increase of the inlet pressure and approached saturation at about 4880 rpm. The low performance of the turbine at low inlet pressure is due to energy loss in the mechanical parts such as the bearing and turbine blades. Generally an impulse turbine has low efficiency at low inlet pressure.

When the exciting current of the alternator was switched on (the turbine was fully loaded), in the first four performance tests (test1 to test4) a rise of inlet pressure by about three times caused the speed of the shaft to increase by more than three times. In the next four tests (test5 to test8) when the inlet pressure was doubled, the rotational speed of the shaft was raised by about 14%. In the last three tests (test 8

to test10), an increase of inlet pressure by 25% raised the turbine shaft speed by more than 2%. It was observed that at low inlet pressure the turbine performance was low. The main reasons could be the frictional losses in the mechanical parts and the high torque needed to overcome the magnetic field in the alternator.

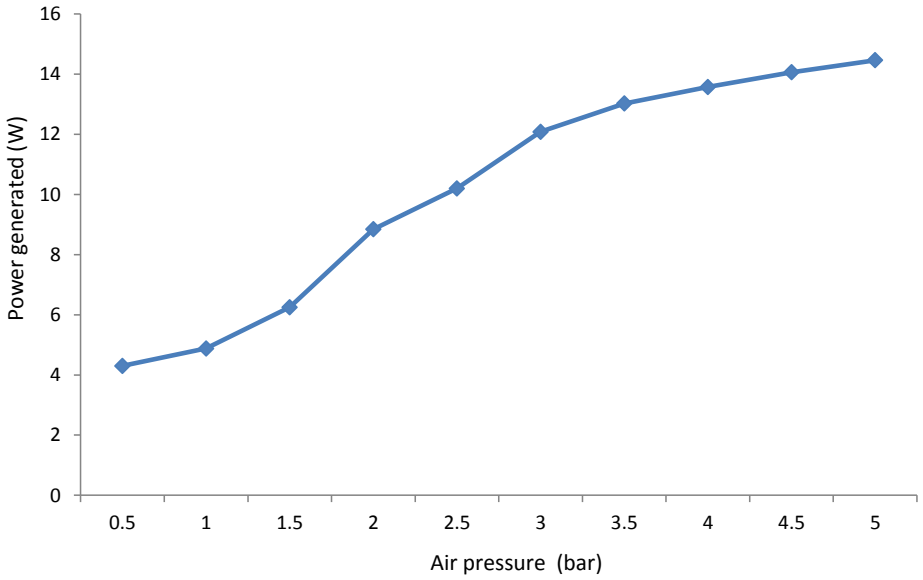

Figure 4.10: Power generated by the turbine with increase in the inlet air pressure

Figure 4.10 shows the variation of the power output against inlet pressure of the model generator driven by the model single stage impulse turbine. The performance of the turbine can be analyzed by dividing the curve into three based on the slope. In the three tests (test1 to test3) the increase of inlet pressure by four times caused the power output to increase by 45%. In the next three tests (test3 to test6) doubling the inlet pressure increased the power output by 93% and for the last three experiments the change in the inlet pressure by three times caused the output to rise by 19.7%. It was observed that at low inlet pressure the output of the model generator was low. This is mainly due to energy loss in the mechanical parts such as the bearing and belt-pulley systems and the high magnetic field in the alternator for which high torque is required

to turn the windings within the magnetic field. However, with the increase in pressure the power output increased steadily.

CHAPTER FIVE

5.0 CONCLUSION AND RECOMMENDATION

5.1 CONCLUSION

The intention of this work was to design and fabricate a model Organic Rankine Cycle (ORC) power plant to utilize the geothermal resource (brine) in Olkaria I geothermal power plant. The main components of the model power plant were designed, fabricated and performance assessment tests of the two heat exchangers and the turbine were conducted. The performances of the heat exchangers were evaluated in terms of the overall heat transfer coefficients, heat energy transferred, and pressure drops across the heat exchangers. It is anticipated that, an efficient and cost-effective ORC power plant can be constructed to utilize the low-grade geothermal brine resources at Olkaria I geothermal power plant to generate electricity.

The design and fabrication methods of the components of the model power plant have proven to be successful in utilizing low temperature heat resources. The main components of the model Organic Rankine Cycle power plant have been fabricated using commercially available materials to overcome the economic barrier. The experiments have produced encouraging results with regard to the performance of each component of the Organic Rankine Cycle power plant operating at low temperature heat resources. Pentane represents an excellent compromise between its thermal properties and environmental considerations.

A fixed tube shell and tube heat exchanger performs satisfactorily for the evaporator of an organic rankine cycle system operating at low temperature. The overall heat transfer coefficient of the heat exchanger was established to be within the standard

range of shell and tube heat exchangers. The overall efficiency of the evaporator was 61% which implies that the heat exchanger is thermally suitable for the evaporator of the model power plant.

The water cooled shell and tube condenser performed adequately for the model organic Rankine cycle system. The overall coefficient for heat transfer of the heat exchanger was found to be within the range of the shell and tube heat exchanger. In addition to this the cooling capacity was greatly improved with increase in cooling water mass flow rate. The shell and tube heat exchanger is thermally suitable for use as the condenser of the model waste heat recovery ORC power plant.

Furthermore, the single stage impulse turbine performed adequately to convert the kinetic energy of gas into mechanical energy (shaft work). The results of the assessment tests revealed that the turbine has the best performance at higher inlet pressures. Moreover, the turbine is compact and has low capital and maintenance costs. Fabrication of the model power plant components locally adds extra economic value to the concept of Organic Rankine Cycle power plant.

5.2 RECOMMENDATIONS FOR FUTURE WORK

The performance assessment tests of the components of the model Organic Rankine Cycle power plant proved that the low temperature geothermal brine heat sources are a promising option. The single row radial deep groove ball bearings were used to support the shaft of the turbine. This type of bearings is general purpose bearings and are not designed for leak tight applications. Design of a gas tight bearing is recommended for future study. Moreover, the cost benefit analysis of the binary cycle power plant should be conducted. and the capital cost of the piping and other equipment are also

recommended for further study as the production wells are scattered.

Working fluid selection is a critical part of the ORC power plant design for the utilization of the low temperature heat source and must consider the economic and environmental effects. The working fluid R-245fa is also environmental friendly its performance should be studied for utilization in a waste heat recovery Organic Rankine Cycle (ORC) power plant.

REFERENCES

[1] *World Energy outlook 2012 Fact sheet, IEA, How will global energy market evolve to 2035 (http://www.worldenergyoutlook.org/media/weowebsite/2012/factsheets.pdf).*

[2] T. E. Bearden Dec. 2007, "Rapid and Decisive Solution of the World Energy Crisis and Global Warming." Slightly updated Feb. 2008.

[3] Clety Bore Kwambai, "Exergy Analysis of Olkaria I Power Plant, KENYA," in *Geothermal Training Programme*, 2005.

[4] M. Mburu, "Geothermal energy utilisation," in *Exploration for Geothermal Resources*, 2009.

[5] Halliburton, "solving challenges, geothermal energy environmental benefits." http://www.halliburton.com/en-US/ps/solutions/clean-energy/geothermal-energy/geothermal-energy-environmental-benefits.

[6] Barbier, E., "Geothermal energy technology and current status: an overview," *Renewable and Sustainable Energy Reviews*, vol. 6(1-2), pp. 3–65, 2002.

[7] Sadiq J. Zarrouk and Hyungsul Moon, "Efficiency of geothermal power plants: A worldwide review," *Geothermics*, vol. 51, pp. 142–153, 2014.

[8] Danielle Kurtzleben, Jan 15, 2014, "Global economic growth will accelerate in 2014," tech. rep., World Bank, 2014.

[9] *Kenya Facts and Figures 2012: Kenya National Bureau of Statistics.*

[10] Pius Kollikho and Benot Rivard, "Harnessing Geothermal Energy: The case of Kenya," tech. rep., LTS International, 2013.

[11] *Expression of Interest (EOI) for Feasibility Study on Binary Power Generation from Brine Produced at Olkaria I & II Power Plants: General information by KENGEN(2012).*

[12] *Improving Geothermal Power Plant Performance by Repowering with Bottoming Cycles: Proceedings of the World Geothermal Congress 2005 Antalya, Turkey, 24-29 April*, 2005.

[13] Mohanty B, Paloso G., "Economic power generation from low-temperature geothermal resources using organic Rankine cycle combined with vapour absorption chiller," *Heat Recovery Systems and CHP* , vol. 12(2), pp. 143–158, 1992.

[14] Imroz Sohel M., "An iterative method for modelling the air-cooled organic Rankine cycle geothermal power plant," *Internation Journal of Energy Res.*, vol. 10, pp. 1002–1015, 2010.

[15] Subbiaha S., Natarajan R., "Thermodynamic analysis of binary-fluid Rankine cycles for geothermal power plants," *Energy Conversion and Management*, vol. 28(1), pp. 47–52, 1988.

[16] Takahisa Yamamoto , Tomohiko Furuhata, Norio Arai and Koichi Mori, "Design and Testing of the Organic Rankine Cycle," *Energy* , vol. 26 , pp. 239–251, 2001.

[17] Huijuan Chen, D. Yogi Goswami, Muhammad M. Rahman, Elias K. Stefanakos, "A supercritical Rankine cycle using zeotropic mixture working fluids for the conversion of low-grade heat into power," *Energy* , vol. 36, pp. 549–555, 2011.

[18] Bahaa Saleh, Gerald Koglbauer, Martin Wendland, Johann Fischer, "Working fluids for low-temperature organic Rankine cycles," *Energy* , vol. 32, pp. 1210–1221, 2007.

[19] "2013 Geothermal Power: International Market Overview, September 2013."

[20] James M. Mariaria, "Response of Olkaria East Field Reservoir to Production." Thirty-Seventh Workshop on Geothermal Reservoir Engineering Stanford University, Stanford, California, January 30 - February 1, 2012 SGP-TR-1949.

[21] *Geothermal Resource Assessment Case Example, Olkaria-I, C. Ofwana*, 2008.

[22] International, "Geothermal overview," tech. rep., international report, 2012.

[23] Peter A. Ouma, "Geothermal Exploration in Keny." Presented at Short Course V on Exploration for Geothermal Resources,at Lake Naivasha, Kenya, October 29-November 19, 2010.

[24] C. G. Denbow, "Pedagogical development and technical research in the area of geothermal power production," Master's thesis, KTH Industrial Engineering and Management, 2011.

[25] J. W. Lund, "Characteristics, Development and Utilization of Geothermal Resources," Oregon Institute of Technology, 2010.

[26] Mahmut Parlaktuna, "Geothermal Reservoir Engineering." Middle East Technical Univeristy, Petroleum and Natural Gas Engineering Department .

[27] *Geothermal Power Plant Cycles and Main Components: Dr. Pll Valdimarsson*, 2011.

[28] Nurdan Yildirim Ozcan, *Modeling, Simulation and Optimization of Flashed-Steam Geothermal Power Plants from the Point of View of Noncondensable Gas Removal Systems.* PhD thesis, The Graduate School of Engineering and Sciences of Izmir Institute of Technology, 2010.

[29] Bodvardson G, Eggers DE., "The exergy of thermal water," *Geothermics*, vol. 1(3), p. 935, 1972.

[30] Stephen Lawrence , "Geothermal Energy," in *presentation*, Leeds School of Business University of Colorado Boulder, CO 80309-0419.

[31] B. Teguh, "Design of n-butane radial inflow turbine for 100 kw binary cycle power plant," *International Journal of Engineering & Technology IJET-IJENS*, vol. 11, p. 06, 2011.

[32] Alessandro Franco, Marco Villani, "Optimal design of binary cycle power plants for water-dominated, medium temperature geothermal fields." Dipartimento di Energetica L. Poggi, Universit di Pisa, Largo Lucio Lazzarino 56126 Pisa, Italy.

[33] Uri Kaplan, "Advanced Organic Rankine Cycles in Binary Geothermal Power Plants," *Ormat Technologies Inc. (http://www.ormat.com)*, vol. 3, pp. 1–8, November 2007.

[34] Alessandro Franco, "Power production from a moderate temperature geothermal resource with regenerative Organic Rankine Cycles," *Energy for Sustainable Development*, vol. 15, pp. 411–419, 2011 .

[35] *Organic Rankine Cycle Configurations*, 2007.

[36] Kanoglu,M., "Exergy Analysis of a dual-level binary geothermal power plant," *Geothermics*, vol. 31, pp. 709–724, 2002.

[37] Kose,R., "Geothermal Energy Potential For Power Generation in Turkey. A case study in Simau, Kutanya.," *Renewable Energy and Sastainable Energy Review*, vol. 11, pp. 497–511, 2007.

[38] Paul Moya, Ronald DiPippo,, "Unit 5 bottoming binary plant at Miravalles geothermal field, Costa Rica: Planning, design, performance and impact," *Geothermics*, vol. 36, pp. 63–96, 2007.

[39] Alessandro Franco, Marco Villani, "The smaller temperature difference between evaporation and condensation indicates that the pressure drop ratio will be much smaller," *Geothermics*, vol. 38, pp. 379–391, 2009.

[40] Musbaudeen Oladiran Bamgbopa, "Modeling and Performance Evaluation of an Organic Rankine Cycle (ORC) With R245fa as Working Fluid ," Master's thesis, Middle East Technical University, Northern Cyprus Campus , 2012.

[41] A. Schuster, S. Karellas, E. Kakaras, H. Spliethoff, "Energetic and economic investigation of Organic Rankine Cycle applications.," *Applied Thermal Engineering*, vol. 29, pp. 1809–1817, 2009.

[42] R. Rayegan and Y., Tao., "A procedure to select working fluids for Solar Organic Rankine Cycles (ORCs).," *Renewable Energy*, vol. 36, pp. 659–670, 2011.

[43] Bertrand F. Tchanche , Gr. Lambrinos, A. Frangoudakis, G. Papadakis, "Low-grade heat conversion into power using organic Rankine cycles A review of various applications," *Renewable and Sustainable Energy Reviews*, vol. 15, pp. 3963–3979, 2011.

[44] Mathias Aarre Maehlum, "How a Geothermal Power Plant Generates Electricity." http://energyinformative.org/how-a-geothermal-power-plant-generates-electricity/.

[45] Umesh Kumar, Munawar N Karimi, Basant K Agrawal, "Optimization and selection of Organic Rankine Cycle for low grade heat recovery by using graph theo-

retical approach." Department of Mechanical Engineering, Faculty of Engineering and Technology, Jamia Millia Islamia, New Delhi, India.

[46] E. K. S. Huijuan Chen, D. Yogi Goswami, "A review of thermodynamic cycles and working fluids for the conversion of low-grade heat," *Renewable and Sustainable Energy Reviews*, vol. 14, pp. 3059–3067, 2010.

[47] Brandon J. Woodland, James E. Braun, Eckhard A. Groll, William Travis Horton, "Performance Benefits for Organic Rankine Cycles with Flooded Expansion," *Publications of the Ray W. Herrick Laboratories*, vol. 6, p. 5, 2010.

[48] R. DiPippo, "Second law assessment of binary plants generating power from low-temperature geothermal fluids," *Geothermics*, vol. 33, pp. 565–586, 2004.

[49] Recurrent Engineering, LLC, "Kalina Cycle Concepts." 2012.

[50] C. J. Bliem, "The Kalina Cycle and Similar Cycles for Geothermal Power Production." Idaho Falls, Idaho 83415.

[51] H.D. Madhawa Hettiarachchi , Mihajlo Golubovic, William M. Worek , Yasuyuki Ikegami, "Optimum design criteria for an Organic Rankine cycle using low-temperature geothermal heat sources," *Energy* , vol. 32 , pp. 1698–1706, 2007 .

[52] Teguh, P. Bambang; Trisno, M. D., "Model of Binary Cycle Power Plant using Brine as Thermal Energy Sources and Development Potential in Sibayak," *International Journal of Electrical & Computer Sciences IJECS-IJENS*, vol. 11, p. 02, 2011.

[53] T. Kuppan, *Heat Exchanger Design Handbook.* Marcel Dekker, Inc, 2000.

[54] F. P. Incropera and D. P. Dewitt, *Introduction to Heat Transfered.* New York, NY, USA, 2006.

[55] R.Thundil, "Shell side numerical analysis of a shell and tube heat exchanger considering the effects of baffle inclination angle on fluid flow," *International Journal of Thermal Science*, vol. 16, no. 4, pp. 1165–1174, 2012.

[56] Ashutosh Maurya, "Turbine Design." Steam Turbine Design (Adapted from E. F. Church, Jr., Steam Turbines, McGraw-Hill, 1950.).

[57] Helmut Pollak, Norbert Thamm, "Design And Materials For Modern Steam Turbines With Two Cylinder Design Up To 700 MW." Siemens AG, Power Generation, Germany.

[58] Akshay Hattiangadi, "Working Fluid Design for Organic Rankine Cycle (ORC) Systems ," Master's thesis, Delft University of Technology, 2013.

[59] Andi J. Nugroho, "Optimization of Electrical Power Production from High-Temperature Geothermal Fields with Respect to Silica Scaling Problems ," Master's thesis, School of Engineering and Natural Sciences, United Nations University, Geothermal Training Programme, 2011.

[60] *Optimum Cycles for Geothermal Power Plants, Paola Bombarda and Ennio Macchi*, 2000.

[61] Henry Wesula, "Olkaria I Geothermal Power Station Operation Challenges." proceedings, Kenya Geothermal Conference 2011 Kenyatta International Conference Center, Nairobi, November 21-22, 2011.

[62] Peter A. Ouma, "Geothermal Exploration and Development of the Olkaria Geothermal Field." Presented at Short Course IV on Exploration for Geothermal Resources,at Lake Naivasha, Kenya, November 1-22, 2009.

[63] Meseret Teklemariam, "Overview of Geothermal Resource Utilization and Potential in East African Rift System." Presented at Short Course III on Exploration for Geothermal Resources, organized by UNU-GTP and KenGen, at Lake Naivasha, Kenya, October 24 - November 17, 2008.

[64] A. Rettig, M. Lagler, T. Lamare, S. Li, V. Mahadea, S. McCallion, J. Chernushevich, "Application of Organic Rankine Cycles (ORC)," in *World Engineers' Convention*, 2011.

[65] Gary Zyhowski and Andrew Brown, "Low Global Warming Fluids for Replacement of HFC-245fa and HFC-134a in ORC Applications," tech. rep., Honeywell, 2011.

[66] *NIST Chemistry Webbook(www.webbook.nist.gov/chemistry).*

[67] Akash Pandey, "Performance Analysis of a Compact Heat Exchanger," Master's thesis, National Institute of Technology Rourkela , 2011.

[68] Sandeep K. Patel, Alkesh M. Mavani, "Shell and Tube Heat Exchanger Thermal Design With Optimization of Mass Flow Rate and Baffle Spacing.," *International Journal of Advanced Engineering Research and Studies*, vol. E-ISSN2249 - 8974., p. 8974, 2012.

[69] Lars J. Brasz and William M. Bilbow, "Ranking of Working Fluids for Organic Rankine Cycle Applications," in *International Refrigeration and Air Conditioning Conference*, 2004.

APPENDIX A

A.1 DESIGN OF TURBINES

Tangential force on a blade

$$F_u = \dot{m}(V_{w1} - V_{w2}) \tag{A.1}$$

(mass flow rate × change in velocity in tangential direction)

or Tangential force on the blade:

$$F_u = \dot{m}\Delta V_w \tag{A.2}$$

Power developed

$$\dot{W} = \dot{m}V_d\Delta V_w \tag{A.3}$$

Fundamental ideal nozzle energy relations

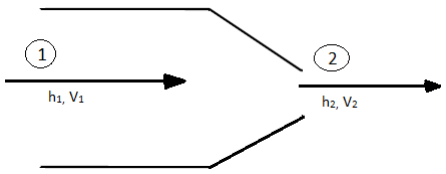

Figure A.1: Flow through nozzle [56]

$$h_1 + \frac{V_1^2}{2} = h_2 + \frac{V_2^2}{2} \Rightarrow \frac{V_2^2 - V_1^2}{2} = h_1 - h_2 \tag{A.4}$$

where V = absolute velocity, h_1 - h_2 = Δh is the available energy.

Consider V_r be the velocity of the vapor relative to the blade. The positive direction is to the right as shown in Figure 2 and 3:

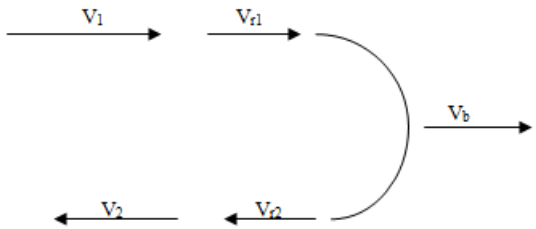

Figure A.2: Velocity diagram of the blade [56]

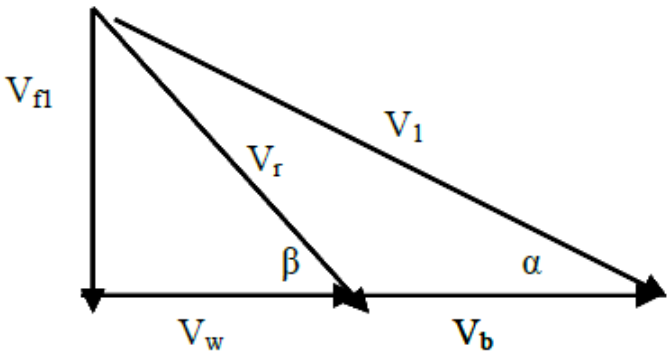

Figure A.3: Schematic of the velocity triangle [56]

$V_1 = V_{r1} + V_b$

$V_2 = V_{r2} + V_b$

Since the blade is frictionless, $V_{r2} = -V_{r1}$, Furthermore, because energy conversion in the blade is complete, $V_2 = 0$. Substituting and combining the two equations:

$V_1 + V_2 = V_{r1} + V_{r2} + 2V_b$

$$V_1 = 2V_b \tag{A.5}$$

Actual nozzle angle

Equation (5), corrected for a finite nozzle angle, α, becomes:

$$V_1 cos\alpha = 2V_b \tag{A.6}$$

Available blade work and power

Assuming steady state and steady flow at the entrance and exit the equation reduces to:

$$T_{shaft} = \dot{m}(rV_{w2} - rV_{w1}) \tag{A.7}$$

Where T_{shaft} is the torque.

The shaft work then is:

$$\dot{W}_{shaft} = \omega T = \dot{m}\omega(rV_{w2} - rV_{w1}) \tag{A.8}$$

But $V_b = \omega r$, Therefore,

$$\dot{W}_{shaft} = \dot{m}V_b(V_{w2} - V_{w1}) \tag{A.9}$$

On a unit mass basis:

$$W_{shaft} = V_b(V_{w2} - V_{w1}) \tag{A.10}$$

Initial conditions of the turbine design

Nozzle angle assumed to be 20^o then:

The inlet conditions:

V_b=5m/s

$(V_1)_{ideal} = \frac{2V_b}{cos20} = \frac{2*5m/s}{cos20} = 10.64m/s$ when increased by 10%: $(V_1)_{ideal} = 11.7m/s$

Table A.1: Initial conditions of the turbine design

Sr. No.	Quantity	Value
1	Power developed at the shaft coupling (kW)	1.85
2	Power generated(kW)	1
3	Generator efficiency	0.7
4	Maximum blade velocity (m/s)	5
5	Initial vapor pressure (bar)	2.5
6	Initial vapor temperature(^{o}C)	54
7	Condenser pressure (bar)	1

The tangential velocity: $V_{w1} = V_1 cos\alpha = 11.7 * cos20 = 11m/s$

relative velocity: $V_{r1} = V_{w1} - V_b = 11 - 5m/s = 6m/s$

Axial Velocity: $V_{f1} = V_1 sin\alpha = 11 * sin20 = 3.76m/s$

$V_{r1} = \sqrt{v_{f1}^2 + v_{r1}^2} = \sqrt{3.76^2 + 6^2} = 7.1m/s$

$\beta = tan^{-1}\frac{V_{f1}}{V_{r1}} = \frac{3.7}{6} = 32^o$

The turbine exit conditions:

Considering $\gamma = \beta = 32^o$

$k_b = (0.892 - 6 * 10^{-5}V_{r1})^{\frac{1}{2}} = (0.892 - 6 * 10^{-5} * 50.5)^{\frac{1}{2}} = 0.943$

$V_{r2} = k_b V_{r1} = 0.943 * 6 = 5.66m/s$

$\gamma = \beta = 32^o$

Tangential velocity: $V_{rw2} = V_{r2} cos\alpha = 5.66 * cos32 = -4.8m/s$

$V_{w2} = V_{rw2} + V_b = -4.8 + 5 = 0.2m/s$

Turbine blade work per unit mass

$w_b = -V_b(V_{w2} - V_{w1}) = -5(-0.2 - 11) = 55J/kg$

Actual energy available to blade

Actual available energy = (A.E) = $\frac{V_1^2}{2} = \frac{82^2}{2} = 3362$J/kg

Turbine blade efficiency

Blade efficiency =$\frac{(W_b)act}{A.E} = \frac{2856}{3362} = 0.85$

Ideal work of the turbine

$$\dot{w}_{act} = \eta_{turb} * \eta_{mech} * \eta_b * \eta_{gen} * \dot{w}_{ideal}$$

$$\dot{w}_{ideal} = \frac{\dot{w}_{act}}{\eta_{turb} * \eta_{mech} * \eta_b * \eta_{gen}} = \frac{1kJ/s}{0.8 * 0.97 * 0.9 * 0.7} = 2kJ/s$$

The ideal power output of the turbine is 2kJ/s.

Isentropic turbine work

Considering the assumptions in Table 3.1, the design process and thermodynamic analysis of the cycle were carried out. For ideal expansion in the turbine, the entropy of

the fluid at the exit of turbine s_2 is the same as that of the fluid at the inlet to the turbine s_1 as shown in the figure 3.2. At a fixed turbine exit pressure and entropy s_1, the enthalpy of the fluid at state 2 (turbine exit) is obtained from table of the thermodynamic properties of pentane. Thus the power output of the turbine ($\dot{W}_t$) equals to :

$$\dot{W}_t = (h_{2s} - h_1) \tag{A.11}$$

From the thermodynamic property table of pentane the enthalpy h_1= 43.383kJ/kg and h_{2s}= -0.03251 kJ/kg

Actual turbine work (w_{act})

The actual work of the turbine(Figure 3.4) is determined by the following equations:

Isentropic work (w_{ideal}) = h_{2s}-h_1= 43.383 kJ/kg - (-0.03252)kJ/kg = 43.4155 kJ/kg

η=$\frac{w_{act}}{w_{ideal}}$ $\Rightarrow$ w_{act}= η_{tur} * η_{mech}*η_{gen}* w_{ideal} = 0.8*0.97*0.7*43.4155 kJ/kg = 23.5833 kJ/kg

The actual turbine work is 23.5833 kJ/kg.

The enthalpy and temperature at state 2 can be determined as follows:

w_{act} = (h_1-h_2) η_{th} = ($\frac{w_{act}}{w_{idea}}$) w_{act} = (η_{th} * w_{idea}) h_1-h_2 = (η_{th} * w_{idea}) $\Rightarrow$ h_2 = h_1-(η_{th} * w_{idea}) = 43.383 - (43.4155*0.8) = 8.65 kJ/kg

Hence h_2 = 8.65 kJ/kg and the corresponding temperature T_2 = 40^{o}C.

Working fluid flow rate

Total power output from turbine($\dot{W}$) = $\dot{m}_{wf}$· w_{act} $\dot{m}_{wf}$ = $\dot{W}/w_{act}$ = $\frac{2kJ/s}{23.583kJ/kg}$ = 0.085 kg/s

Ideal work of the turbine

$$\dot{W}_t = h_{2s} - h_1 \tag{A.12}$$

From the thermodynamic property table of pentane the enthalpy h_1= 43.383 kJ/kg and h_{2s}= -0.03251 kJ/kg

Actual turbine work (w_{act})

The actual work of the turbine(Figure 5) is determined by the following equations:

Isentropic work (w_{ideal}) = h_{2s}-h_1= 43.383 kJ/kg - (-0.03252) kJ/kg = 43.4155 kJ/kg

$\eta = \frac{w_{act}}{w_{ideal}} \Rightarrow w_{act} = \eta_{tur} * \eta_{mech} * \eta_{gen} * w_{ideal}$ = 0.8∗0.97∗0.7∗43.4155 kJ/kg = 23.5833 kJ/kg

The actual turbine work is 23.5833 kJ/kg.

The enthalpy and temperature at state 2 can be determined as follows:

$w_{act} = (h_1\text{-}h_2)\ \eta_{th} = (\frac{w_{act}}{w_{idea}})\ w_{act} = (\eta_{th} * w_{idea})\ h_1\text{-}h_2 = (\eta_{th} * w_{idea}) \Rightarrow h_2 = h_1\text{-}(\eta_{th} * w_{idea})$ = 43.383 - (43.4155∗0.8) = 8.65 kJ/kg

Hence h_2 = 8.65 kJ/kg and the corresponding temperature T_2 = 40^{o}C.

Working fluid flow rate

Total power output from turbine ($\dot{W}$) = $\dot{m}_{wf} \cdot w_{act}$

$\dot{m}_{wf} = \dot{W}/w_{act} = \frac{2kJ/s}{23.583kJ/kg}$ = 0.085 kg/s

Fabrication of the turbine

Casting of the turbine blades and rotor:

The blades and rotor are the main component of the turbine. Each part was cast separately using sand casting. The pattern for the blade was prepared in a semi-cylindrical shape of 15 mm radius and 50 mm height. It also has an extruded part (flange), of trapezoidal shape, on the bottom part. The flange has a bases of 18 mm and 10 mm, height of 20 mm and thickness of 10 mm. The flange was fitted and fastened in to the groove provided on the rotor.

Similarly, the pattern for the rotor was prepared in a cylindrical shape of 100 mm diameter and 18 mm height. It comprised twelve grooves of trapezoidal shape on the top side, to accommodate the flange of the turbine.

Two wooden frames, lower molding flask (the drag) and upper molding flask (the cope), without fixed top or bottom were made to accommodate the mold as shown in Figure. The frames were square of size 20 cm by 20 cm. A smooth wooden board also used to support the pattern from the bottom was placed securely on the floor. The drag was located after positioning the pattern properly on the board in such a way that at least 8 cm gap was left between the pattern and the sides of the drag. Fine and clean facing sand (to ensure smooth surface) was placed over the pattern. The sand was made to be very fine and clean in order to attain smooth surfaces. After striking the mold in the flask using a wooden bar, the drag was drawn across the top surface to remove the excess sand. The second flask, the cope was then placed upside down of the drag and clamped together using a joint to resist the tendency of float of the cope or shift as the molten alloy fills the cavity. A fine and clean sand was sieved again in the pattern to fill the second flask, the cope.

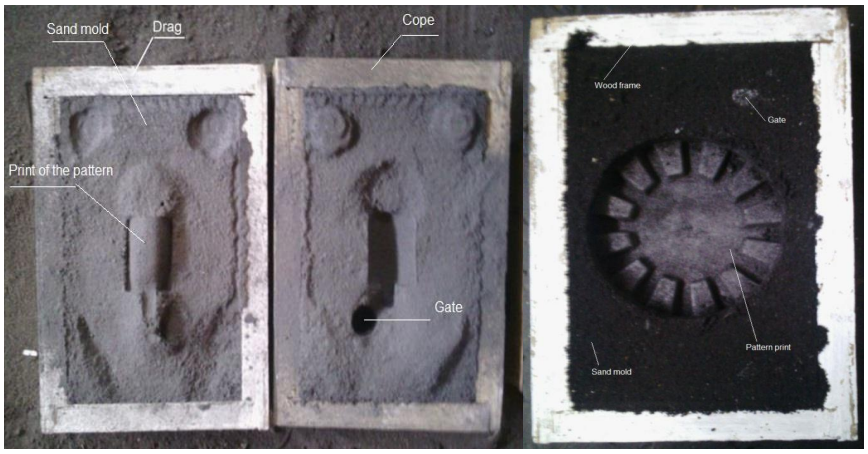

Figure A.4: The pattern print of rotor in the sand mold

The sand was then rammed solidly using the wooden bar and numerous small vent holes were made, through the sand mold before removing the pattern, to ensure the escape of gases from the molten metal. The flasks were separated to remove the pattern and after tapping the pattern slightly to loosen it from the mold, it was removed and exact shaped cavity was printed in the mold on to which the molten metal was poured (Figure). Two channels, the gate and the riser, were drawn on the mold through which the molten metal enters the mold cavity and molten aluminum was placed to feed the casting as it shrinks, respectively.

The next day the mold was further dried using CO_2 while aluminum alloy was melted in the furnace. The cope and drag were clamped together in the same configurations using a joint to resist the tendency of the cope to float or shift as the molten alloy flows to fill the cavity. The molten aluminum alloy was then poured in the mold cavity through the gate provided on the mold. The casting was removed from the mold after the molten metal solidified and cooled to ambient conditions.

Figure A.5: The pattern and cast of the rotor and blade

Casting of the turbine casing

The turbine casing was designed to accomplish four main objectives. It provides housing for the turbine, accommodates a suitable position of nozzle, provides exhaust gas passage to condenser and supports the shaft. The high pressure vapor from evaporator flows into the casing and was directed to the turbine blade through the nozzle. The turbine shaft is designed to be supported by two bearings that would be housed in the casing.

Figure A.6: Wooden pattern of the casing and sand core for the cavity of the turbine casing

The pattern making of the turbine casing (Figure 10) was done in two parts, the core preparation for the internal feature or cavity and pattern preparation of the outer

contour. The pattern for the outer contour was made in two pieces known as split type pattern to avoid the difficulties of pattern removal from the molding and minimize destruction of the mold edges. Each pattern is then accommodated in different mold called the upper mold (cope) and lower part of the mold (drag). The patterns were made with pins known as Dewel pin to keep the alignment between the two parts of the pattern.

Core preparation (Figure 11) is a complex procedure. It was made by mixing fine grained white sand, molasses and sodium silicate to form a solid sand core. Molasses is a breaking agent which helps easy break down of the core after casting. Unlike many core binders available, sodium silicate has a distinct advantage because the cores can be made at room temperature without baking in an oven. This allows the cores to be made in simple core boxes. Mixing of sand, molasses and sodium silicates was done in an open area by hand. The treated sand was then packed in a wooden core box, which contains a cavity in the shape of the internal features of the casing.

The core box was made from wood in a similar way to the split type pattern. The well mixed dry-sand, breaking agent and binder was packed into the box and struck by a wooden bar and then scraped level with the top. Small vent holes at many points through the sand core were created in which CO_2 gas was then applied to the sand through these holes from a low pressure cylinder to activate the sodium silicate to bind the sand. The vent holes also assist to increase the porosity of core which act as paths for gases to escape. The two core boxes were flipped over and the core segment drops out of the core box.

APPENDIX B

B.1 EVALUATION OF THE THERMAL PARAMETERS FOR THE HEAT EXCHANGERS

Evaporator Sizing and Rating

During the heat transfer process energy is conserved therefore for the cold and hot fluid:

$$Q_h = Q_c = Q = C_h(T_{hi} - T_{ho}) = C_c(T_{co} - T_{ci}) \tag{B.1}$$

where heat capacity rate for hot or cold fluid $C = \dot{m}c_p$ and c_p is specific heat at constant pressure.

using eq(3.4) and c_p average=4.1818 kJ/kgk

$Q_{1-2} = (\dot{m}C_p(T_{hi} - T_{ho}))_{water} = 0.1 * 4.181(54 - 36) = 7.5258kJ/s$

$Q_{1-2} = (\dot{m}C_p)_{wf}(T_{co} - T_{ci}) \Rightarrow T_{co} = T_{ci} + \frac{Q}{(\dot{m}C_p)_{wf}} = 25 + \frac{7.5258}{0.12*2.385} = 51^o\text{C}$

$\Delta T_1 = T_{hi} - T_{co} = 54 - 51 = 3^o\text{C}$

$\Delta T_2 = T_{ho} - T_{ci} = 36 - 25 = 11^o\text{C}$

The log mean temperature difference for counter flow shell tube heat exchanger is given by:

$$\Delta T_{lm,cf} = \frac{(T_{hi} - T_{co}) - (T_{ho} - T_{ci})}{\ln[\frac{(T_{hi} - T_{co})}{(T_{ho} - T_{ci})}]} \tag{B.2}$$

$\Delta T_{lm} = \frac{\Delta T_1 - \Delta T_2}{\ln(\frac{\Delta T_1}{\Delta T_2})} = \frac{3-11}{\ln(\frac{3}{11})} = 6.157^o\text{C}$

Heat exchanger surface area:

$A_s = \frac{Q_{1-2}}{U\Delta T_{lm}} = \frac{87525.8}{(3000*6.157)} = 0.41\text{m}^2$

Total length of the copper tube:

$L = \frac{A_s}{\pi D} = \frac{0.41}{\pi * 0.01} \simeq 13.1$ m

$N_t = \frac{A_s}{\pi D l} = \frac{0.41}{\pi * 0.01 * 0.4} = 33$

where N_t is the number of tubes in the shell and l is the length of single tube inside the shell.

The details of the design and core dimensions of the evaporator are summarized in Table 3.5.

Condenser sizing and rating

$$Q_{2-3} = \dot{m} C_p \Delta T \tag{B.3}$$

$Q_{2-3} = \dot{m} C_p \Delta T = 0.09 kg/sec * 2.385 kJ/kg.K * (51 - 25) K = 5.5809 kJ/sec$

Heat transfer to the cooling fluid:

Using eqn 3.8 and assuming C_p remains constant:

$(Q_{2-3} = \dot{m} C_p \Delta T)_{water} = \dot{m} C_p (T_{co} - T_{ci})$

$T_{co} = T_{ci} + \frac{Q_{2-3}}{\dot{m} C_p} = 20 + \frac{5.55809}{0.3 * 4.1818} = 24^o$C

$\Delta T_1 = T_{hi} - T_{co} = 51 - 24 = 27^o$C

$\Delta T_2 = T_{ho} - T_{ci} = 25 - 20 = 5^o$C

Log mean temperature difference for counter flow shell and tube heat exchanger is given by:

$$\Delta T_{lm,cf} = \frac{(T_{hi} - T_{co}) - (T_{ho} - T_{ci})}{\ln[\frac{(T_{hi} - T_{co})}{(T_{ho} - T_{ci})}]} \tag{B.4}$$

$\Delta T_{lm} = \frac{\Delta T_1 - \Delta T_2}{\ln(\frac{\Delta T_1}{\Delta T_2})} = \frac{27-5}{\ln(\frac{27}{5})} = 13^o$C

Heat transfer surface area:

$Q = UA_s\Delta T_{lm} \Rightarrow A_s = \frac{Q}{U\Delta T_{lm}} = \frac{5.5809kJ/s}{1630*13} \approx 0.2634m^2$

The total length of copper tube:

$L = \frac{Q}{\pi D} = \frac{0.2634}{\pi*0.01} \approx 8.4$ m

The length of tube in the shell is 40 cm i,e l= 40 cm.

The number of tubes in the shell (N_t):

$N_t = \frac{A_s}{\pi DL} = \frac{0.2634}{\pi*0.01*0.40} = 21$

where N_t is the number of tubes in the shell.

Evaporator Test one

1. Heat Duty of the evaporator(Q_1):

$$Q_1 = C_c(T_{co} - T_{ci}) = \dot{m}C_p\Delta T = AUT_{LMTD}$$

$$Q_1 = \dot{m}C_p(T_{co} - T_{ci})$$

$$Q_1 = 0.12(2.385)(47.8 - 28.5) = 5523.66W$$

For counter flow heat exchanger the heat duty (Q) is given by $Q = AUT_{LMTD}$ Where

$\mathrm{T}_{LMTD} = \frac{((T_{wi}-T_{po})-(T_{wo}-T_{pi}))}{ln((\frac{(T_{wi}-T_{po}}{T_{wo}-T_{pi}}))}$

$\Delta T_1 = T_{hi} - T_{co}$=52.9-47.8=5.1 k

$\Delta T_2 = T_{ho} - T_{ci}$= 35.7-28.5= 7.2 k

2. The log mean temperature difference (T_{LMTD})

$\mathrm{T}_{LMTD} = \frac{(\Delta T_1-\Delta T_2)}{ln(\frac{\Delta T_1}{\Delta T_2})} = \frac{(5.1-7.2)}{ln(\frac{5.1}{7.2})} = 6.09$ k

3. Overall heat transfer coefficient (U_1)

$Q_1 = AU_1T_{LMTD} \Rightarrow U_1 = \frac{Q_1}{AT_{LMTD}} = \frac{5523.66}{(0.41)(6.09)} = 2212.21$ (W/m^{2}K)

The performance parameters of the five tests are evaluated and summarized in the

table below.

Table B.1: Evaluated values of performance parameters of the evaporator

Parameter	**Test 1**	**Test 2**	**Test 3**	**Test 4**	**Test 5**
LMTD (K)	6.09	5.75	5.86	5.63	5.54
Heat Duty (W)	5523.66	5732.09	5801.24	5867.1	5895.72
Overall heat tr. coeff (W/m^{2}K)	2212.21	2413.69	2504.54	2543.54	2595.633

Condenser test one

1. Heat Duty (Q_1) of the condenser $Q_{con} = C_c(T_{co} - T_{ci}) = \dot{m}C_p\Delta T = AUT_{LMTD}$

$Q_{con} = \dot{m}C_p(T_{hi} - T_{ho}) = Q_{con} = 0.12(2.385)(47.8 - 29) = 5380.56$ W

For counter flow heat exchanger the heat duty (Q) is given by $Q = AUT_{LMTD}$ Where

$\mathrm{T}_{LMTD} = \frac{((T_{wi}-T_{po})-(T_{wo}-T_{pi}))}{ln((\frac{(T_{wi}-T_{po}}{T_{wo}-T_{pi}}))}$

$\Delta T_1 = T_{hi} - T_{co}$= 47.8 - 23.6 = 24.2 k

$\Delta T_2 = T_{ho} - T_{ci}$= 29 - 23.5 = 5.5 k

2. The log mean temperature difference (T_{LMTD})

$\mathrm{T}_{LMTD} = \frac{(\Delta T_1-\Delta T_2)}{ln(\frac{\Delta T_1}{\Delta T_2})}$= $\frac{(24.2-5.5)}{ln(\frac{24.2}{5.5})}$ = 12.62 k

3. The overall heat transfer coefficient (U)

$Q = AUT_{LMTD} \Rightarrow U = \frac{Q}{AT_{LMTD}} = \frac{5380.56}{(0.2634)(12.62)} = 1618.65$ W/m^2 K

The performance parameters of the five tests are evaluated and summarized in the table below.

Table B.2: Evaluated values of performance parameters of the condenser

Parameter	**Test 1**	**Test 2**	**Test 3**	**Test 4**	**Test 5**
LMTD (K)	12.62	12.95	12.99	13	13.09
Heat Duty(W)	5380.56	5523.66	5552.28	5580.9	5609.52
Overall heat tr. coeff(W/m^{2}K)	1618.65	1619.35	1622.73	1629.84	1638.2

APPENDIX C

C.1 EVAPORATOR EXPERIMENTAL TEST RESULTS

Table C.1: Experimentally observed data of the evaporator

Parameter	**Test 1**	**Test 2**	**Test 3**	**Test 4**	**Test 5**
Hot water					
Pressure in (kPa)	110	110	110	110	110
Pressure out (kPa)	108.5	108.2	107.5	107.2	106.5
Pressure drop (kPa)	1.1	1.8	2.5	2.8	3.5
Flow rate (kg/sec)	0.16	0.18	0.2	0.22	0.24
Temperature in (^{o}C)	52.9	52.9	52.8	52.8	52.6
Temperature out (^{o}C)	35.7	35.9	36.0	36.2	36.2
Working fluid (Pentane)					
Pressure in (kPa)	150	150	150	150	150
Pressure out (kPa)	148.7	148.5	148.2	148.1	147.6
Pressure drop (kPa)	1.3	1.5	1.8	2.0	2.4
Flow rate (kg/s)	0.12	0.12	0.12	0.12	0.12
Temperature in (^{o}C)	28.5	28.4	28.5	28.4	28.3
Temperature out (^{o}C)	47.8	48.5	48.7	48.9	48.9

APPENDIX D

D.1 EXPERIMENTALLY OBSERVED DATA OF THE CONDENSER

Table D.1: Experimentally observed data of the condenser

Parameter	**Test 1**	**Test 2**	**Test 3**	**Test 4**	**Test 5**
Pentane					
Pressure in (kPa)	148.7	148.5	148.2	148.1	147.6
Pressure out (kPa)	138.2	137.9	137.2	137.1	136.6
Flow rate (kg/sec)	0.12	0.12	0.12	0.12	0.12
Temperature in (^{o}C)	47.8	48.5	48.7	48.7	48.9
Temperature out (^{o}C)	29.0	29.2	29.3	29.2	29.3
LMTD (K)	12.6215	12.925	12.8703	12.838	12.925
Cooling water					
Pressure (kPa)	250	250	250	250	250
Flow rate (kg/s)	0.15	0.2	0.25	0.30	0.35
Temperature in (^{o}C)	23.5	23.5	23.6	23.6	23.6
Temperature out (^{o}C)	23.6	23.6	23.9	23.8	23.8

APPENDIX E

E.1 PERFORMANCE TEST RESULTS OF THE TURBINE

Table E.1: Experimental results of the turbine

Test No.	Pressure (bar)	No load RPM	Loaded RPM	Power (W)
1	0.5	1917	1585	4.34
2	1.0	3305	2051	4.88
3	1.5	3952	2912	6.256
4	2.0	3952	3922	8.835
5	2.5	4556	3934	10.206
6	3.0	4692	4064	12.08
7	3.5	4745	4169	13.02
8	4.0	4812	4458	13.5
9	4.5	4830	4546	14.06
10	5.0	4880	4590	14.46